

An-Najah National University

Faculty of Graduate Studies

**The optical band and optical constants of non-
crystalline WO₃ thin films doped with Ti
deposited by dip coating in sol-gel**

By

Manar Ibraheem Ali Shwahna

Supervisor

Dr. Iyad Saadeddin

Co-Supervisor

Dr. Mohammed Suleiman

**This Thesis is Submitted in Partial Fulfillment of the Requirements for
the Degree of Master of physics, Faculty of Graduate Studies, An-
Najah National University, Nablus, Palestine.**

2015

The optical band and optical constants of non-crystalline WO₃ thin films doped with Ti deposited by dip coating in sol-gel

By

Manar Ibraheem Ali Shwahna

This Thesis was defended successfully on 20/8/2015 and approved by:

Defense Committee Members

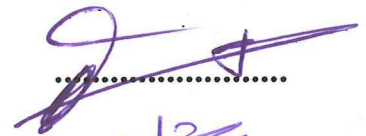
1. Dr. Iyad Saadeddin / Supervisor

2. Dr. Mohammed Suleiman / Co-Supervisor

3. Prof. Atef Qasrawi / External Examiner

4. Prof. Ghassan Safarini/ Internal Examiner

Signature


.....


.....


.....


.....

Dedication

أهدي عملي هذا لله سبحانه و تعالى
و أسأله أن يقبله خالصا لوجهه الكريم

I dedicate my dissertation work purely to the lord (Allah) his

Glorified and Exalted with full of majesty, full of honor

O Allah, I am asking you to accept my work purely for you

Acknowledgement

After thanking Allah, who gave me the ability and the patience to accomplish this thesis, I would like to thank my dear Mother and Father, who provided me with psychological support and encouragement. Also my honest thanks go to my husband Ahmad for his continues encouragement, support and patience during the study period.

With all respect and appreciation I like to thank: Dr. Iyad Saadeddin for all his guidance, understanding, support , and Dr. Mohammed Suleiman for his scientific support, encouragement, guidance and constructive advice.

Also my sincere thanks go to my doctors Prof. Dr. Atef Qasrawi for his help, sound advice in all aspects of my research work and support during my study, and for his technical help like doing the spectroscopy measurements in AAUJ physics laboratories, data analysis, and moral support during research work and thesis writing

I appreciate help and support from all members of the Chemistry Department at An-Najah National University especially laboratory technician, in particular Mr. Nafiz Dweikat and Anas Ali.

Thanks to my brothers and sisters with all my love. I also would like to express my sincere gratitude to Miss Khayriah Hamarsheh for her support that she provides different facilities through my job to complete my study.

Manar Shwahna

الإقرار

أنا الموقع أدناه موقع الرسالة التي تحمل العنوان:

The optical band and optical constants of non-crystalline WO₃ thin films doped with Ti deposited by dip coating in sol-gel

أقر بأن ما اشتملت عليه الرسالة هو نتاج جهدي الخاص، باستثناء ما تمت الإشارة إليه حيثما ورد، وأن هذه الرسالة ككل، أو أي جزء منها لم يقدم من قبل لنيل أي درجة أو لقب علمي أو بحثي لدى أي مؤسسة تعليمية أو بحثية أخرى.

Declaration

The work provide in this thesis, unless otherwise referenced, is the researcher's own work, and has not been submitted elsewhere for any other degree or qualification.

Student's name:

اسم الطالبة: منار إبراهيم علي سويهد

Signature:

التوقيع: منار إبراهيم

Date:

التاريخ: 2015 / 8 / 20

Table of Contents

No.	Subject	Page
	Dedication	III
	Acknowledgements	IV
	Declaration	V
	Table of Contents	VI
	List of Tables	VIII
	List of Figures	IX
	Abstract	XI
	Chapter 1: Introduction	1
1.1	Why WO ₃ based thin film?	1
1.2	Previous Studies	3
1.3	Objectives of this work	5
	Chapter 2: Theoretical Background	6
2.1	Optical Properties	6
2.1.1	The electromagnetic radiation nature	6
2.1.2	Maxwell's Equations	8
2.1.3	The Electromagnetic Wave Equations In The Vacuum	8
2.1.4	The Electromagnetic radiation propagation In The matter	10
2.1.5	Refractive Index (n) and the dielectric constant (ϵ)	14
2.1.6	Fresnel's Equations	16
2.1.6.1	Boundary conditions	17
2.1.6.2	Derivation of Fresnel's equations	19
2.2	The Energy band gap (E _g)	26
2.2.1	Introduction to the band gap E _g	26
2.2.2	The Absorption Of The light In Matter	29
2.2.3	Measuring The Optical Band Gap Technique	31
2.2.4	Dispersion	32
2.3	Deposition techniques of WO ₃ -based thin films	37
2.3.1	Sputtering deposition	38
2.3.2	Spin coating techniques	39
2.3.3	Vacuum Evaporation	40
2.3.4	Sol-Gel Process	41
2.3.5	Dip coating	42
	Chapter 3 : Experimental Work	44
3.1	Material and film preparation	44
3.1.1	Chemicals and Solvents	44
3.2	Preperation of the thin films	44
3.2.1	Substrate Cleaning Process	44
3.2.2	Preparation the WO ₃ Sol-gel solution doped with Ti	45
3.2.3	Preparation the WO ₃ : Ti thin films by coating method	47

3.3	Measurements	49
3.3.1	X-Ray Diffraction (XRD)	49
3.3.2	Transmittance and reflectance	50
	Chapter 4: Results and Discussion	51
4.1	X-Ray diffraction (XRD)	51
4.2	The Transparency (T)	52
4.2.1	The coefficient (α)	53
4.2.2	The Energy gap (E_g)	54
4.3	The Reflectance (R)	60
4.3.1	The dielectric constant (ϵ)	62
4.3.2	The thicknesses of investigated films	64
4.4	The oscillator parameters	66
	Conclusions	71
	References	73
	الملخص	ب

List of Tables

No.	Subject	Page
3.1	List of intended compositions, WCl_6 and $TiCl_2$ mass used in sol-gel preparation.	46
4.1	The optical energy band gap values of doped $WO_3:Ti$ thin film at different concentrations of Ti.	59
4.2	Variation of the dielectric constant of WO_3 thin film, doped with different concentrations of Ti at specific wavelengths.	63
4.3	The calculated thickness of WO_3 thin film doped with Ti at different concentration of Ti	65
4.4	The dispersion energy E_d , the oscillator energy E_0 , the lattice dielectric constant ϵ_L and the static refractive index ϵ_s of WO_3 thin films doped with Ti at different concentrations.	68

List of Figures

No.	Subject	Page
2.1	The electromagnetic radiations	7
2.2	The reflection law	11
2.3	All the Interactions of the electromagnetic radiation with any matter	12
2.4	The refractive process	14
2.5	The series polarization of the light	20
2.6	The parallel polarized light.	23
2.7	The conduction and the valence bands in conductor, semiconductor and insulator.	27
2.8	(a) Electrons (solid dots) occupy the (V.B) (b) electrons leave holes in (V.B) when they travel from to (C.B)	28
2.9	Types of energy band gap (a) direct (b) indirect	30
2.10	Sputtering processes	38
2.11	spin coating stages.	40
2.12	Vacuum evaporation technique	41
2.13	Dip coating technique steps	43
3.1	ultrasonic vibrator	48
3.2	Local designed and manufactured dip coater designed at physics department by Mr. Mohammad Bahjat and Dr .Iyad Saadeddin.	48
3.3	WO ₃ :Ti thin films deposition steps.	49
4.1	XRD patterns of Ti doped WO ₃ thin films prepared at different Ti concentration with non doped WO ₃ film (10%, 20%, 30% and 40%) in comparison .	52
4.2	The transparency (T) data for WO ₃ thin films doped with different concentrations of Ti.	53
4.3	Variation of absorption coefficient as function of incident photon energy for WO ₃ films doped with different concentrations of Ti .	54
4.4	Plots of $(\alpha E)^{1/p}$ as function of E for p values being 2 (a), 1/2 (b), 3 (c) and 3/2 (d) for WO ₃ thin films doped with 10% Ti .	56
4.5	The plot of $(\alpha E)^2$ as function of E for (Ti non-doped) WO ₃ thin film	57
4.6	The plot of $(\alpha E)^2$ as function of E for WO ₃ :Ti doped thin films at deferent concentrations of Ti.	58
4.7	The variation of the energy gap of WO ₃ thin films doped with different Ti concentration and undoped.	59
4.8	The reflectance (R) spectra for WO ₃ doped with Ti at	61

	different concentrations	
4.9	The variation of reflectivity of WO ₃ thin films doped with Ti as a function of Ti concentration.	62
4.10	The relation between dielectric constant of WO ₃ :Ti doped thin film with the concentration of Ti at certain wavelengths. .	63
4.11	The reflectance (R) spectra for WO ₃ doped with 10 % Ti .	65
4.12	The value of $\frac{1}{n(E)^2-1}$ as a function of E ² of WO ₃ thin film at different Ti concentrations	67
4.13	The value of n ² versus λ ² of WO ₃ :Ti doped thin film at specific concentrations	70

The optical band and optical constants of non-crystalline WO₃ thin films doped with Ti deposited by dip coating in sol-gel

By

Manar Ibraheem Ali Shwahna

Supervisors

Dr. Iyad Saadeddin

Dr. Mohammed Suleiman

Abstract

The optical constants and optical band gaps of the non-crystalline tungsten oxide (WO₃) thin films doped with Ti deposited by dip coating method onto glass substrates with different atomic concentrations of Ti have been investigated by optical characterization method. The films were annealed at 160°C to guarantee maximum transparency. The amorphous crystal structure of the as grown and annealed films were revealed by XRD. The optical data of WO₃ thin film have revealed a direct allowed transition band gap of 3.1 eV, which increases slightly up to 3.6 eV by increasing Ti concentration due to the formation of TiO₂ new phase that may be introduced within the amorphous structure. The effect of Ti concentration on the film thickness and optical constants (refractive index, absorption coefficient and dielectric constants) of these films has been also investigated. The films thickness was found to increase with increasing doping concentration from 0.373 to $\approx 0.7\mu\text{m}$ due to the increase in the liquid viscosity, as expected. The room temperature refractive index, which was calculated from the reflectance and transmittance data, allowed the identification of the dispersion and oscillator energies lattice dielectric constant and static dielectric constant of these films, which show that WO₃ thin films doped with Ti can be used as UV sensors, where 10% Ti doping is the best sensor.

Chapter One

Introduction

1.1 Why WO₃ based thin film?

After Deb' s discovery of the electrochromism behavior of tungsten oxide (WO₃) thin films [1] , WO₃ has been one of the most popular transition metal oxide because of its wide interesting electrochromic, optochromic and gasochromic properties particularly in thin film form [2]. WO₃ thin films have been prepared by various deposition processes like thermal evaporation [3], chemical vapor deposition [4], spraying [5], laser deposition [6], sputtering [7], sol-gel dip coating [8], spin coating technique [9], recently hot filament metal oxide deposition (HFMOD) and hot filament chemical vapor deposition (HFCVD) [10].

WO₃ has complex phase transitions which are presenting a rich temperature and pressure dependent phase sequence, and a perovskite-like structure based on the corner sharing of WO₆ octahedra. With regard to the ideal cubic perovskite type, the symmetry of WO₃ is lowered resulting from two distortions: (1) tilting of WO₆ octahedra and (2) displacement of tungsten from the core of its octahedron [11]. Pure WO₃ crystals exhibit at least five polymorphs in the temperature range varying from absolute zero to melting point at 1700 K, monoclinic (δ and γ phase), triclinic, orthorhombic, tetragonal [12], each of these structural transformations exhibits different electrical, optical and magnetic behaviors which attracted the attention of researchers over the past few years to explore their

potential scientific and technological applications in the fields of display systems and microelectronics [13]. The WO_3 porous films with a large surface area enable the analytes to diffuse through where this kind of films may be used in sensing functions [14], also amorphous WO_3 can be used in optical and electrical sensors due to its high photochromic and electrochromic sensitivity which results from its high surface area [15].

WO_3 in the nano-fibers shape express high response and recovery characteristics to NH_3 [16,17], also WO_3 in the nano shape were used to prevent infection occurring on the surface of prostheses by an innovative approach [18].

Doping WO_3 thin films with different compounds and ions open the door to other new applications. For example doping WO_3 with MgO increases its photocatalyst properties which can be used in producing hydrogen from the decomposition of H_2O [19], TiO_2/WO_3 composite materials have been reported as fascinating ones: high active photocatalyst, photocatalytically inactive materials, energy storage photocatalyst [20,21]. WO_3 treated by NH_3 can be used to increase the efficiency of solar cells [22]. Recently, some studies have shown a wide range of WO_3 thin films' different applications include high energy density microbatteries [23,24], selective catalysis, microelectronics, electro-catalysis, and optoelectronics [25], sensitive and fast sensors for different gases H_2 [26], H_2S [27], NH_3 [28], O_3 [29], CO [30].

It is known that WO_3 films can change their optical transmittance upon the insertion or the extraction of charge . This property made them of critical

importance for electrochromic device technology, such as for dynamic or “smart” windows that are at the forefront of emerging energy-saving advances in building technologies [31]. As well as, for multilayer devices like (WO₃/Ag/WO₃) multilayer transparent anode which founded to be the most suitable transparent anode in the polymer light emitting diodes (PLEDs) [32].

1.2 Previous Studies

Interest in the physical, optical and electrical properties of transition oxide family has sharply grown during the past few years. Due to their importance in many applications in science and technology [33], so a huge number of studies had investigated the different structures of tungsten oxide .

In particular there is a lack of knowledge about the structure of WO₃ below room temperature. Sibuyi have studied the crystal structure of WO₃ at room temperature and below, using neutron powder diffraction that he found a mixture of γ and δ -WO₃ at 25°C, but when the sample was cooled to room temperature, he found pure δ -WO₃ [34]. S. Walia et al found that above 130 K and below 223 K a monoclinic low-temperature modification α -WO₃ and at higher temperatures a triclinic β -modification occurs, but it converts to another monoclinic γ -WO₃ shape stable between 290 K and 603 K, while between 603K and 973 K, WO₃ has orthorhombic symmetry [33]. C. V. Ramana et. al. [35] investigated the phase transformation in WO₃ thin films by annealing from 30° C to 500° C and concluded that the phase transition that thin films occur in sequence as the temperature is

increased : monoclinic to orthorhombic to hexagonal. Recently I. Jimenez et. al. said that the crystal structure of WO_3 thin films stay monoclinic until the annealing temperature become 400°C , and above this temperature the structure will change to a triclinic one [36].

The crystal structure of WO_3 also can be changed by doping with specific materials. C. V. Ramana and co-workers recently revealed an amorphous phase of WO_3 when doped with (10%) Ti concentration, and mixed WO_3 – TiO_2 (monoclinic δ - WO_3 and rutile TiO_2) phases at higher Ti concentration [37]. The x-ray diffraction results found the solid solution WNb_2O_8 phase with mixed WO_3 – Nb_2O_5 (monoclinic ε - WO_3 and orthorhombic Nb_2O_5) phases at lower Nb concentration (2%) and mixed WO_3 – Nb_2O_5 phases at higher Nb concentrations (6 and 10%) [38]. A modification was carried out for WO_3 by doping MgO led to interestingly photocatalyst [39]. Doping WO_3 thin films with Ti was found to increase their photocatalyst properties and 2% Ti was found to be the best effective one, this was the result founded by [40]. On the other hand, deposition of gold nanoparticles onto the surface of WO_3 thin film enhanced the photochromism of the film. This result may be helpful in technical application and provide a more detailed understanding of photochromic mechanism [41].

Doping WO_3 thin films with 10 % Ti produces completely granular and coarse without fibrous network films. Where the cycle stability, charge and storage capacity of these films are improved by doping. However, coloration efficiency decreases [42].

The crystallization of WO_3 lowered by doping Ti with low concentration which causes an increase in their electrochromic performance, and they will obtain superior electrical conductivity and reaction kinetics, i.e. the times of bleaching and coloration in WO_3 :Ti doped films are much less than those of un-doped WO_3 [43].

Recent studies [44] were able to develop gas sensor based on WO_3 thin film doped with different amount of Platinum (Pt) or gold (Au) or Palladium (Pd) exhibits acceptable electrochromism behavior.

1.3 Objectives of this work

- 1- Preparation of different WO_3 films doped with Ti with different doping concentrations WO_3 :Ti (0 - 40 %) by dip-coating technique in sol-gel .
- 2- Studying the optical properties of the prepared thin films.
- 3- Studying the structural properties of the prepared thin films.
- 4- Studying the dielectric properties of the prepared thin films.

The dependence of the physical properties of the thin films on the amount of Ti doped will be investigated using :

X-ray diffraction (XRD) analysis,

UV-VIS spectroscopy,

Studying of the refractive,

Dielectric constant calculations,

Film thickness measurements,

Energy gap calculations and

Oscillator parameters calculations.

Chapter Two

Theoretical Background

2.1 Optical Properties

To understand the optical properties of any material we must refer to electromagnetic radiation theory. Where the interaction of the electromagnetic waves with the material, through specialized devices like the spectrometer, yields an important data if analyzed using different processes, we can understand everything about optical properties of that materials.

2.1.1 The electromagnetic radiation nature

The nature of the electromagnetic radiation was not clear and confused the scientists for many centuries, that many scientists proved the corpuscular nature of the light, while others advocated a wave nature. But Einstein had proved by his famous photoelectric effect experiment that the electromagnetic radiation has the dual nature , i.e. wave and corpuscular nature. He also discovered the "Photon" (also called a quanta of energy ; it is an elementary zero mass particle sometimes behaves like a particle other times like a wave) [45,46].

Electromagnetic radiation is a form of energy, it is characterized by transverse wave through the space which consists of alternating combination of time dependent electric and magnetic field perpendicular to each other and to the direction of propagation [47]. The electromagnetic spectrum includes a great range of wavelengths, where each certain part of

this spectrum represents one type of rays. Fig. (2.1) shows all ray types. They have essentially the same phenomenon that they travel through space and have similar interaction effects on matter [48]. But, they differ in the wavelength which causes many differences in their properties. For example the human eye can see the visible one but can't see the other parts, and the radio waves are used in the broadcasting. Some materials absorb ultraviolet waves and emit it again as a visible light this process called the fluorescence, so ultraviolet can be used in the tracing. Gamma rays have the most damaging effect, that it can be used to kill the cancer cells. Microwaves are used in the microwave cooker to heat or cook the food [49].

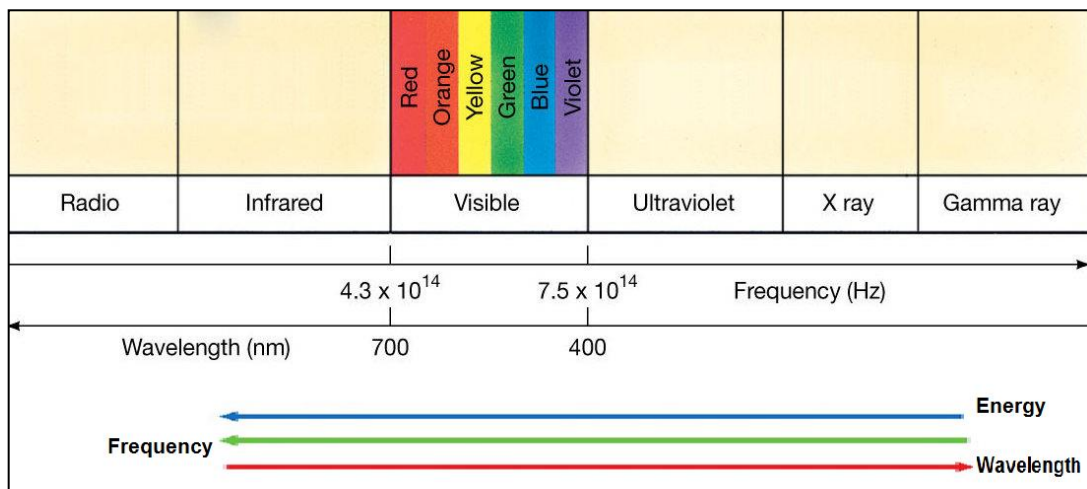


Fig 2.1: The electromagnetic radiations [after 50].

The electromagnetic radiation is usually described by the relation between three factor as shown in the equation [50] :

$$E = h \nu = \frac{hc}{\lambda} \quad (2.1)$$

Where E is the energy of the electromagnetic radiation, ν is its frequency which is proportional to the inverse of its wavelength (λ), h is plank's constant and c is the speed of light.

2.1.2 Maxwell's Equations

James Maxwell expected the entity of the magnetic field, that he described how the electric and the magnetic fields behave and described the relation between them. In the two decades after Maxwell's death, Oliver and Hertz introduced four equations and called them "Maxwell's equations". These four equations summarized the current displacement concept by Maxwell which complete the electromagnetic theory [51-53]. Maxwell's equations were written in differential form as follows [52-54] :

$\nabla \cdot \mathbf{E} = \frac{\rho}{\epsilon_0}$	(i)	
$\nabla \cdot \mathbf{B} = 0$	(ii)	
$\nabla \times \mathbf{E} = -\frac{\partial \mathbf{B}}{\partial t}$	(iii)	(2.2)
$\nabla \times \mathbf{B} = \mu_0 \mathbf{J} + \mu_0 \epsilon_0 \frac{\partial \mathbf{E}}{\partial t}$	(iv)	

Where \mathbf{E} : the electric field, \mathbf{B} : magnetic field, ρ is the charge density, \mathbf{J} is the conduction current density, ϵ_0 and μ_0 are the permittivity and the permeability of free space respectively.

2.1.3 The Electromagnetic Wave Equations in Vacuum

In vacuum where there is no charge or current, it is easy to show that electromagnetic waves can exist there. We set $\rho = 0$ and $\mathbf{j} = 0$ in equations (2.2(i-iv)), they become [55, 56],

$\nabla \cdot \mathbf{E} = 0$	(i)	
$\nabla \cdot \mathbf{B} = 0$	(ii)	
$\nabla \times \mathbf{E} = -\frac{\partial \mathbf{B}}{\partial t}$	(iii)	(2.3)
$\nabla \times \mathbf{B} = \mu_0 \epsilon_0 \frac{\partial \mathbf{E}}{\partial t}$	(iv)	

Taking the curl of equation (iii) and use equation (iv) as follows [55,56],

$$\nabla \times (\nabla \times \mathbf{E}) = -\nabla \times \left(\frac{\partial \mathbf{B}}{\partial t} \right) = -\frac{\partial (\nabla \times \mathbf{B})}{\partial t} \quad (2.4)$$

$$\nabla \times (\nabla \times \mathbf{E}) = -\frac{\partial (\mu_0 \epsilon_0 \frac{\partial \mathbf{E}}{\partial t})}{\partial t} = \mu_0 \epsilon_0 \frac{\partial^2 \mathbf{E}}{\partial t^2} \quad (2.5)$$

Now let's use BAC-CAB formula $\mathbf{A} \times (\mathbf{B} \times \mathbf{C}) = \mathbf{B} (\mathbf{A} \cdot \mathbf{C}) - (\mathbf{C} \cdot \mathbf{A})\mathbf{B}$ to find the value of $\nabla \times (\nabla \times \mathbf{E})$ as follows,

$$\nabla \times (\nabla \times \mathbf{E}) = \nabla (\nabla \cdot \mathbf{E}) - (\nabla \cdot \nabla)\mathbf{E} = \nabla (\nabla \cdot \mathbf{E}) - \nabla^2 \mathbf{E} \quad (2.6)$$

Finally Eqs.(2.5) becomes,

$$\nabla^2 \mathbf{E} = \mu_0 \epsilon_0 \frac{\partial^2 \mathbf{E}}{\partial t^2} \quad (2.7)$$

Which is called the electromagnetic wave equation for \mathbf{E} . Note that equations in (2.3) are symmetric in \mathbf{E} and \mathbf{B} except for the factor of $\mu_0 \epsilon_0$ and a minus sign. If we again repeat the previous steps starting with equation (iv) then use (iii) we will end up with exactly the same wave equation for \mathbf{B} [55,56]

$$\begin{aligned}\nabla^2 \mathbf{B} &= \\ &= \mu_0 \epsilon_0 \frac{\partial^2 \mathbf{B}}{\partial t^2}\end{aligned}\quad (2.8)$$

The speed of \mathbf{E} and \mathbf{B} together is called the speed of electromagnetic waves in vacuum (usually denoted by c), which is equal to the value of the square root of the inverse right hand side factor of equation (2.7) or (2.8) [55,56],

$$c = \frac{1}{\sqrt{\mu_0 \epsilon_0}} \quad (2.9)$$

As $\mu_0 = 1.2566370614 \times 10^{-6} \text{ T} \cdot \frac{\text{m}}{\text{A}}$ and

$\epsilon_0 = 8.854 187 817 \dots \times 10^{-12} \text{ F/m}$,

So $c \cong 3 \times 10^8 \text{ m/s}$

2.1.4 The Electromagnetic radiation propagation in matter

The study of the interaction of electromagnetic radiation with matter is called the spectroscopy, which is very useful in the study of the optical properties of materials. As we said previously, electromagnetic radiation is really just a form of energy 'photons', that exhibit both waves and particles and propagate as electromagnetic waves in the space . These photons can interact with charged particles in the matter (solid, liquid, or gas). Charged particles (electrons or ions) experience Lorentz force when exposed to electromagnetic radiation [57].

The interaction of the electromagnetic waves with any material is controlled by several conditions such as the physical state (solid, liquid, or

gas), the chemical compositions and the crystal structure of that material. When electromagnetic radiation strike a sample of any material, many phenomena may happen (Fig. 2.2); electromagnetic radiation may reflect from the surface, transmitted through the sample and scattered, refracted or absorbed through it, and samples may emit the absorbed energy in a process called fluorescent [58].

The reflection can be described by the reflectivity coefficient as follows [59],

$$R = \frac{\text{power of reflected beam}}{\text{power of incident beam}} \quad (2.10)$$

Reflection law states that when the incident beam strikes the surface (Fig.(2.3)) at θ_i angle with the normal of the surface , it must be reflected with angle θ_r , by the following condition [60] ,

$$\theta_i = \theta_r \quad (2.11)$$

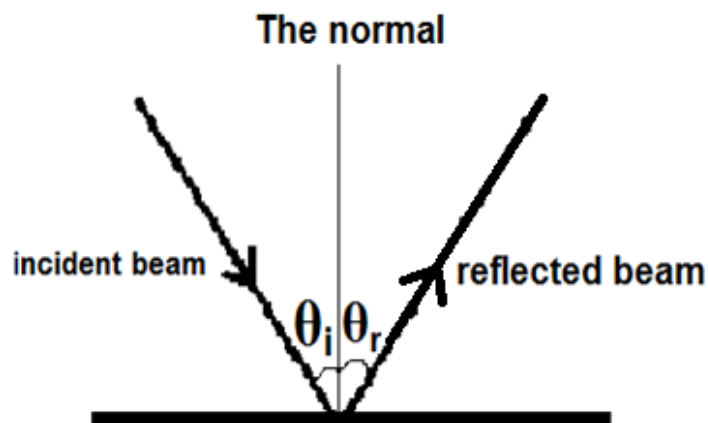


Fig 2.2 : The reflection law [60].

The transmission is also described by coefficient of transmissivity (T) as follows [59]

$$T = \frac{\text{power of transmitted beam}}{\text{power of incident beam}} \quad (2.12)$$

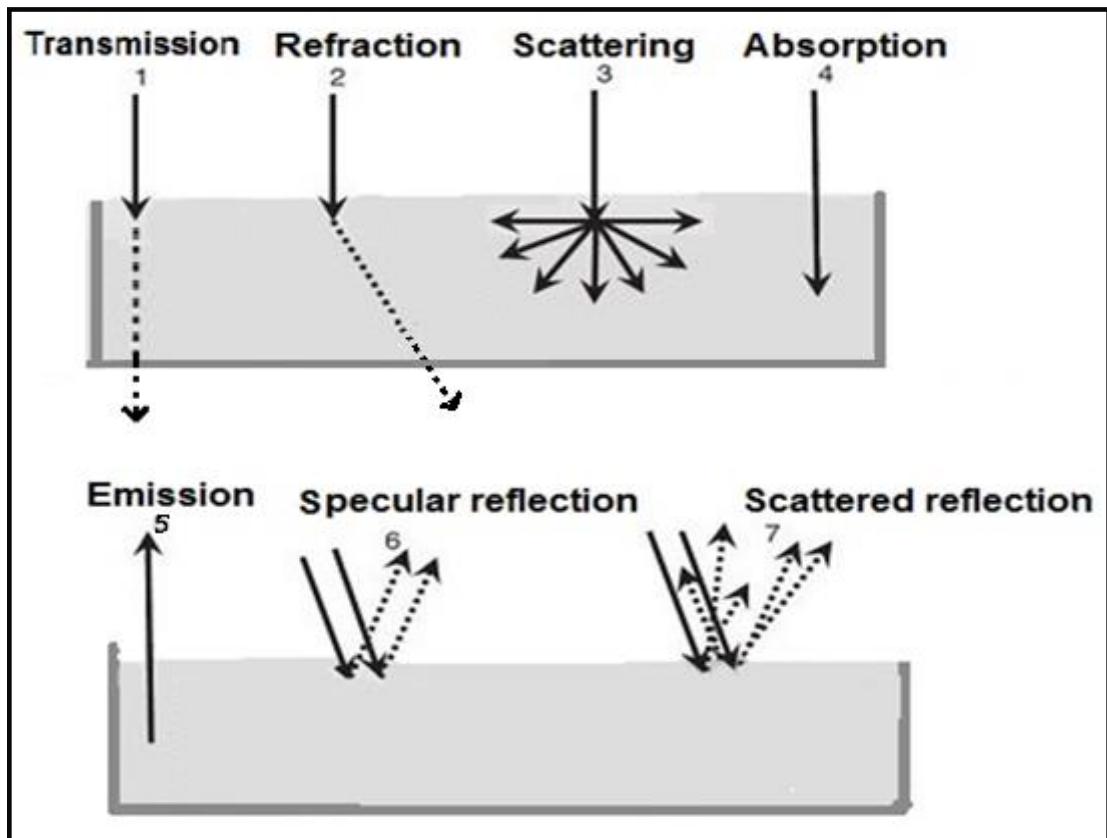


Fig 2.3: All the Interactions of the electromagnetic radiation with any matter [59].

An absorption will occur if the frequency of the incident photons is resonant with the transition frequencies of the atoms in the material.

Atoms, molecules, electrons and ions exist only in specific quantized energy states that any transition between them must be provided with a specific energy (ΔE) equals the difference between the two states according to [61],

$$E_f - E_i = \Delta E = h\nu = \frac{hc}{\lambda} \quad (2.13)$$

The transmission of the medium is clearly related to the absorption, because only unabsorbed waves will be transmitted. Hence, absorption provides a clear picture of the sample's energy level distribution, which helps to understand the electronic and vibration properties of that sample. Indeed, due to differences between materials, each material will absorb certain frequencies differ from any other material. The uniqueness isn't only in the absorbed or emitted frequencies but also in the degree of absorption or emission which is called the intensity. The spectrum (the set of the absorbed or transmitted frequencies with their intensities) of any given sample is the basis for the use of spectroscopy for identification of composition, chemicals, etc.. Quantitatively, absorption can be usually studied by measuring the absorption coefficient (α) [62].

The interaction in which the velocity of the electromagnetic wave changes and change its direction, when propagates through a sample without changing its intensity, is called refraction. This interaction is described by Snell's law of refraction [60,63],

$$n_1 \sin \theta_1 = n_2 \sin \theta_2 \quad (2.14)$$

This law states that if a beam of electromagnetic radiation propagate, at angle θ_1 , with the normal, from a material whose refractive index is n_1 , to other material that has refractive index n_2 , then the refractive beam will travel at θ_2 with respect to the normal, as shown in figure (2.4).

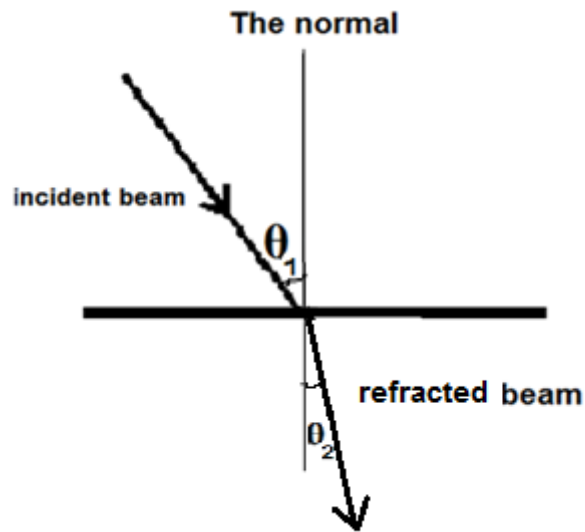


Fig 2.4: The refractive process [60].

Scattering occurs when the electromagnetic waves change their direction and possibly also their frequency without changing their intensity. In this interaction, although the total number of photons is still the same, the photons going in the forward direction decrease because of the direction changing of the incident beam. There are two scattering types, the first is the elastic which happens if there is no energy exchange between the incident photons and the material. While if the diffused photons have different energy than those of income ones, the scattering called inelastic [62].

2.1.5 Refractive Index (n) and the dielectric constant (ϵ)

As indicated before, when the electromagnetic waves is incident at a surface, separates two transparent mediums, some will reflected while the most ratio will refracted and it will suffer a change in its velocity through the new medium. The velocity of the beam in the medium and its

propagation depends on the refractive index. The unitless refractive index, n , is defined as [64],

$$n = \frac{c}{v} \quad (2.15)$$

where c and v are the velocity of the propagating wave in free space and its velocity in the medium respectively.

From equations (2.3) we find that $c = \frac{1}{\sqrt{\mu_0 \epsilon_0}}$, in the same way we can conclude that the velocity of the waves in the medium (v) will be,

$$v = \frac{1}{\sqrt{\mu \epsilon}} \quad (2.16)$$

So,

$$n = \sqrt{\frac{\mu \epsilon}{\mu_0 \epsilon_0}} \quad (2.17)$$

In most nonmagnetic optical media, the magnetic permeability μ is very close to μ_0 and hence we can write Eq. (2.17) as

$$n = \sqrt{\frac{\epsilon}{\epsilon_0}} = \sqrt{\epsilon_r} \quad (2.18)$$

The ratio between the permittivity of a substance and that of free space is called the relative permittivity (the dielectric constant ϵ_r). Relation (2.18) is very important because it relates the dielectric of a material to its optical properties [65]

In materials, the electromagnetic wave experiences attenuation, during its propagation due to various loss mechanisms such as free carrier absorption, generation of phonons (lattice waves), photogeneration and scattering. Due to this, the refractive index becomes a complex function of the electromagnetic wave's frequency and it is denoted by n^* as follows [58],

$$n^* = n + ik \quad (2.19)$$

Where the real part , n , is the refractive index, and the imaginary part, k , is called extinction coefficient.

Also the dielectric permittivity becomes a complex function, and can be written as [58],

$$\varepsilon^* = \varepsilon_r + i\hat{\varepsilon}_r \quad (2.20)$$

In which the real part , ε_r , is called the dielectric constant and the imaginary part, $\hat{\varepsilon}_r$, is the loss factor.

2.1.6 Fresnel's Equations

When the light strikes the surface of a matter, both reflected and refracted waves are produced where they have a direction given by the 'Law of Reflection', equation (2.11), and Snell's law (2.14) respectively. And because these laws don't tell information about the reflected and the transmitted fraction of the incident wave but this information was first provided by Fresnel in 1827. Fresnel equations are derived by assuming that the plane wave solutions on either sides of the boundary satisfy certain boundary conditions [66] .

2.1.6.1 Boundary conditions

The boundary indicate what happen to the electric and magnetic field vectors as they cross the boundary between two different mediums [3].

To introduce the boundary conditions, we must recall Maxwell's equations (2.2), that they will give four boundary conditions. We will start with the integral form of the first one (2.2 a) is [67.68]

$$\oiint \vec{E} \cdot \vec{dA} = \frac{\rho}{\epsilon_0} \quad (2.21)$$

$$\epsilon_0 \oiint \vec{E} \cdot \vec{dA} = \rho \quad (2.22)$$

In dielectric materials there are no free charges that $\rho = 0$, and from equation (2.18) we have to modify ϵ_0 by $\epsilon_r \epsilon_0$. Hence equation (2.22) becomes,

$$\epsilon_r \epsilon_0 \oiint \vec{E} \cdot \vec{dA} = 0 \quad (2.23)$$

This equation implies that if the electromagnetic wave move between two dielectric medias, at an interface, the normal components of the electric field on either sides of the interface are equal,

$$\epsilon_1 E_{n1} = \epsilon_2 E_{n2} \quad (2.24)$$

Which is the first boundary condition.

The integral form of the third Maxwell's equation (2.2 c) is,

$$\oint \mathbf{E} \cdot d\mathbf{l} = -\frac{\partial \Phi_{\mathbf{B}}}{\partial t} \quad (2.25)$$

This yields that the tangential component of the electric field is continuous across the interface,

$$E_{t1} = E_{t2} \quad (2.26)$$

Which is the second boundary condition.

The integral form of the second Maxwell's equation (2.2 a) is,

$$\oiint \vec{\mathbf{B}} \cdot \vec{d\mathbf{A}} = 0 \quad (2.27)$$

This equation implies again the normal components of the magnetic field on either sides of the interface are equal,

$$B_{n1} = B_{n2} \quad (2.28)$$

Which is the third boundary condition.

Finally the last Maxwell's equation (2.2d) can be written in the integral form as,

$$\oint \mathbf{B} \cdot d\mathbf{l} = \mu_0 \mathbf{I} + \mu_0 \epsilon_0 \frac{\partial \Phi_{\mathbf{E}}}{\partial t} \quad (2.29)$$

Where \mathbf{I} is the electrical current (the flow of electrons), here $\mathbf{I} = 0$ because we are talking about dielectrics which have no free electrons also we must convert μ_0 into μ (permeability of medium). Equation (2.29) become as follow,

$$\begin{aligned} & \frac{1}{\mu} \oint \mathbf{B} \cdot d\mathbf{l} \\ & = \varepsilon_0 \frac{\partial \varphi_E}{\partial t} \end{aligned} \quad (2.30)$$

This equation implies again the tangential components of the magnetic field on either sides of the interface are equal,

$$B_{t1} = B_{t2} \quad (2.31)$$

This relation with (2.24), (2.26) and (2.28) are the four boundary conditions.

2.1.6.2 Derivation of Fresnel's equations

There are two different Fresnel's equation depending on the polarization of the incident beam. According to these two cases we will discuss Fresnel equations [69]:

1. The incident beam is polarized with its electric field perpendicular to the plane of incident, the wave is said to be s-polarized (series polarized lights) or TE (transverse electric filed) .
2. The incident beam is polarized with its electric field parallel to the plane of incident, this wave is described as p-polarized (parallel polarized lights) or TM (transverse magnetic field).

a. Derivation of the Fresnel's interface complex-amplitude reflection coefficients R_s , for s-polarization of light

Below in figure 2.5, is an illustration for an incident light comes from a medium with index of refraction n_1 , and passed through a dielectric

material of n_2 , where (θ_i) , (θ_r) , (θ_t) are the angles of incident, reflection and refraction respectively [70].

Here in this case, we assume that the electric field vector is in somewhere on the plane perpendicular to the incident direction plane (plane of paper). The magnetic field that associated with E field, will always have its components perpendicular to electric field, as shown in figure 2.4.

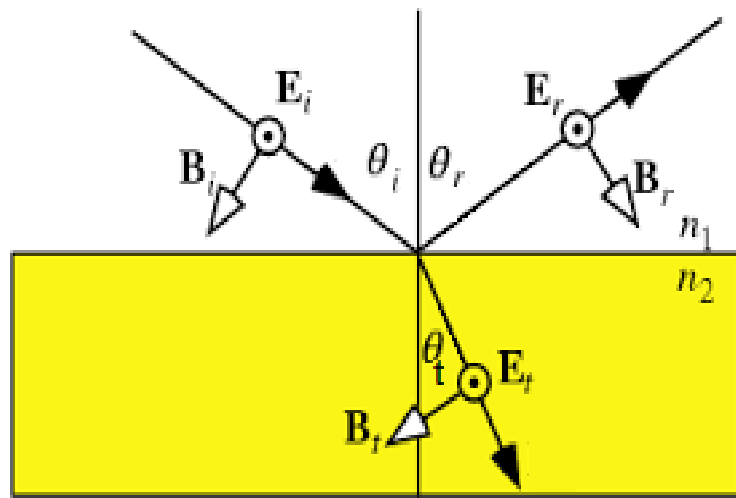


Fig 2.5: The series polarization of the light.

The magnetic field of the incident beam can also be resolved into two components parts, the horizontal component B_h , and the vertical component B_v [68,69],

$$B_h = B \cos \theta_i \quad (2.32)$$

$$B_v = B \sin \theta_i \quad (2.33)$$

Where θ_i is the angle of the incident.

Components of B field for reflected or transmitted beam are the same except for the angle θ_i , which must be θ_r for reflected beam and θ_t for transmitted one.

In section 2.1.6.1, we defined four boundary conditions. Now if we apply 2.26 and 2.28, we can get that,

$$E_i + E_r = E_t \quad (2.34)$$

$$B_i \cos \theta_i - B_r \cos \theta_r = B_t \cos \theta_t \quad (2.35)$$

Under assumption of $\rho = 0$, one can have [71]

$$B = \frac{n}{c} E \quad (2.36)$$

Hence, equation 2.35 become as,

$$n_1 E_i \cos \theta_i - n_1 E_r \cos \theta_r = n_2 E_t \cos \theta_t \quad (2.37)$$

By the law of reflection (2.11) we can set that $\theta_i = \theta_r$, also by using equation (2.34), equation (2.37) become as,

$$n_1 E_i \cos \theta_i - n_1 E_i \cos \theta_i = n_2 (E_i + E_r) \cos \theta_t \quad (2.38)$$

$$n_1 E_i \cos \theta_i - n_1 E_r \cos \theta_i = n_2 E_i \cos \theta_t + n_2 E_r \cos \theta_t \quad (2.39)$$

$$E_i (n_1 \cos \theta_i - n_2 \cos \theta_t) = E_r (n_1 \cos \theta_i + n_2 \cos \theta_t) \quad (2.40)$$

According to equation (2.10),

$$R_s = \left| \frac{(n_1 \cos \theta_i - n_2 \cos \theta_t)}{(n_1 \cos \theta_i + n_2 \cos \theta_t)} \right|^2 \quad (2.41)$$

By eliminating θ_t using Snell's law, and some trigonometric relations, we can write R_s ,

$$R_s = \left| \frac{n_1 \cos \theta_i - \sqrt{n_2^2 - (n_1 \sin \theta_i)^2}}{n_1 \cos \theta_i + \sqrt{n_2^2 - (n_1 \sin \theta_i)^2}} \right|^2 \quad (2.42)$$

Which is Fresnel's equation for the series polarized lights case.

b. Derivation of the Fresnel's interface complex-amplitude reflection coefficients R_p , P-polarization of light

In this polarization case the magnetic field vector and the incident plane will be perpendicular to each other, as shown in figure (2.5). Hence, the electric field vector of the incident light can be resolved into two parts, the horizontal component E_h , and the vertical component E_v [68,69]:

$$\begin{aligned} E_h \\ = E \cos \theta_i \end{aligned} \quad (2.43)$$

$$\begin{aligned} E_v \\ = E \sin \theta_i \end{aligned} \quad (2.44)$$

Now we can apply the boundary conditions, equ's (2.24) and (2.31), on the magnetic field to get that,

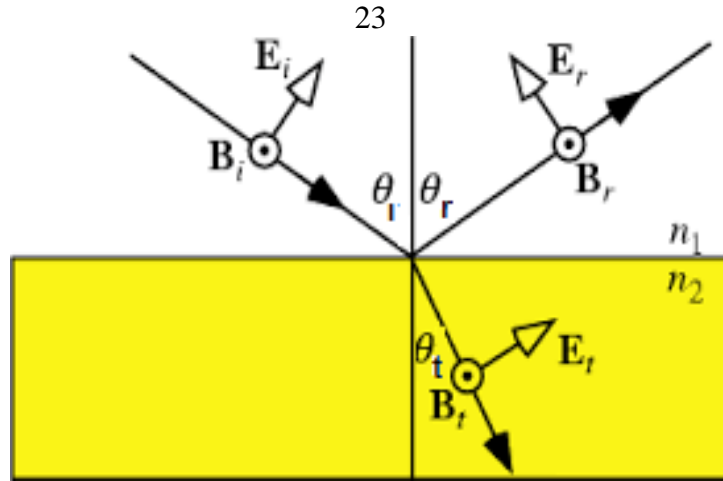


Fig 2.6: The parallel polarized light.

$$B_i + B_r = B_t \quad (2.45)$$

$$E_i \cos \theta_i - E_r \cos \theta_r = E_t \cos \theta_t \quad (2.46)$$

By applying equation (2.36) on (2.45) yields that,

$$E_t = \frac{n_1}{n_2} (E_i + E_r) \quad (2.47)$$

Now substituting (2.47) in (2.46) results that,

$$E_i \cos \theta_i - E_r \cos \theta_r = \frac{n_1}{n_2} (E_i + E_r) \cos \theta_t \quad (2.48)$$

$$n_2 E_i \cos \theta_i - n_2 E_r \cos \theta_i = n_1 (E_i + E_r) \cos \theta_t \quad (2.49)$$

$$n_2 E_i \cos \theta_i - n_2 E_r \cos \theta_i = n_1 E_i \cos \theta_t + n_2 E_r \cos \theta_t \quad (2.50)$$

$$E_i (n_2 \cos \theta_i - n_1 \cos \theta_t) = E_r (n_2 \cos \theta_i + n_1 \cos \theta_t) \quad (2.51)$$

$$R_p = \left| \frac{E_r^{\parallel}}{E_i^{\parallel}} \right|^2 = \left| \frac{(n_2 \cos \theta_i - n_1 \cos \theta_t)}{(n_2 \cos \theta_i + n_1 \cos \theta_t)} \right|^2 \quad (2.52)$$

Also we can eliminate θ_t for p- polarized light so that R_p can be rewritten as,

$$R_p = \left| \frac{n_1 \sqrt{1 - \left(\frac{n_1}{n_2} \sin \theta_i\right)^2} - n_2 \cos \theta_i}{n_1 \sqrt{1 - \left(\frac{n_1}{n_2} \sin \theta_i\right)^2} + n_2 \cos \theta_i} \right|^2 \quad (2.53)$$

Which is Fresnel's equation for the parallel polarized lights.

Finally, the total reflection as known will contain an equal amount of both polarization. Hence, the reflectance will be,

$$R = \frac{R_s + R_p}{2} \quad (2.54)$$

c. The relation between R_s and R_p in a special case, $\theta_i=45^\circ$

In our experiment, there are many special cases first we sent the electromagnetic radiation to the investigated sample in the air ($n_1 \cong 1$), and we measured the reflectivity spectra at 45° angle of incident. Now as $\varepsilon = n_2^2$ and by some trigonometric identities, R_s and R_p equations become [72],

$$R_s = \frac{\cos \theta_i - (\varepsilon - \sin^2 \theta_i)^{\frac{1}{2}}}{\cos \theta_i + (\varepsilon - \sin^2 \theta_i)^{\frac{1}{2}}} \quad (2.55)$$

$$R_p = \frac{\varepsilon \cos \theta_i - (\varepsilon - \sin^2 \theta_i)^{\frac{1}{2}}}{\varepsilon \cos \theta_i + (\varepsilon - \sin^2 \theta_i)^{\frac{1}{2}}} \quad (2.56)$$

Now to relate the R_s and R_p , we can eliminate ε between equation (2.55) and (2.56) by assuming that ,

$$z = (\varepsilon - \sin^2 \theta_i)^{\frac{1}{2}} \quad (2.57)$$

So these equations become,

$$R_s = \frac{\cos \theta_i - z}{\cos \theta_i + z} \quad (2.58)$$

$$R_p = \frac{(z^2 + \sin^2 \theta_i) \cos \theta_i - z}{(z^2 + \sin^2 \theta_i) \cos \theta_i + z} \quad (2.59)$$

From equation (2.58) we can write that,

$$z = \frac{(1 - R_s) \cos \theta_i}{(1 + R_s)} \quad (2.60)$$

By substituting equation (2.59) into (2.60) we obtain that,

$$R_p = R_s \frac{(R_s - \cos 2\theta_i)}{(1 - R_s \cos 2\theta_i)} \quad (2.61)$$

The previous equation represents the relation between R_p and R_s at the same angle of incidence θ_i . It is clear that it is independent of the two media that define the interface and it is also applicable throughout the entire electromagnetic spectrum.

At $\theta_i = 45^\circ$, equation (2.61) reduces to ,

$$R_p = R_s^2 \quad (2.62)$$

Thus the dielectric constant can be studied by using equations (2.54) and (2.62) that we obtain the following equation,

$$R_s^2 + R_s + 2R = 0 \quad (2.63)$$

This equation will have two solutions both solutions are used in equation (2.55), we will have two square equations again. Hence, four possible

solutions were obtained for ε . Only one solution gives an acceptable values for ε which is,

$$\varepsilon = \left(4 + \frac{\sqrt{(16 - 4((Rs - 1)/(Rs + 1))^2)}}{((Rs - 1)/(Rs + 1))^2} \right) \quad (2.64)$$

Where,

$$R_s = \left(-\frac{1}{2} + \sqrt{(0.25 + 2 \times \frac{R}{100})} \right) \quad (2.65)$$

2.2 The Energy band gap (E_g)

2.2.1 Introduction to the band gap E_g

According to the energy bands theory of solids when the isolated atoms form the crystal they collect to each other and their levels of the outer-shells electrons merge into energy bands of closely spaced energy states where electrons are allowed to be present. There are three main kinds of energy bands:

First: the conduction (C.B), the band which contains electrons which are not bounded to the crystal and move freely through the crystal, these electrons usually contribute in the electrical conductivity.

Second: the valance band (V.B) which is filled with electrons which can't contribute in the electrical conductivity.

Third: the energy band gap (E_g) which is a forbidden gap separates between the previous two bands [73,74].

The classification of materials to the three physical states (conductor, semiconductor or insulator) depends on the electrons distribution in the allowed energy bands and the size of the band gap figure (2.6). If the valance electrons fill one or more than (V.B) exactly and leave other (C.B) empty with large energy gap (4-12 eV) the crystal must be an insulator, while if the energy gap is small ($< 4\text{eV}$) it must be considered as a semiconductor, and it must be a conductor if the (V.B) is partially filled with electrons which are already exist in the (C.B) [74].

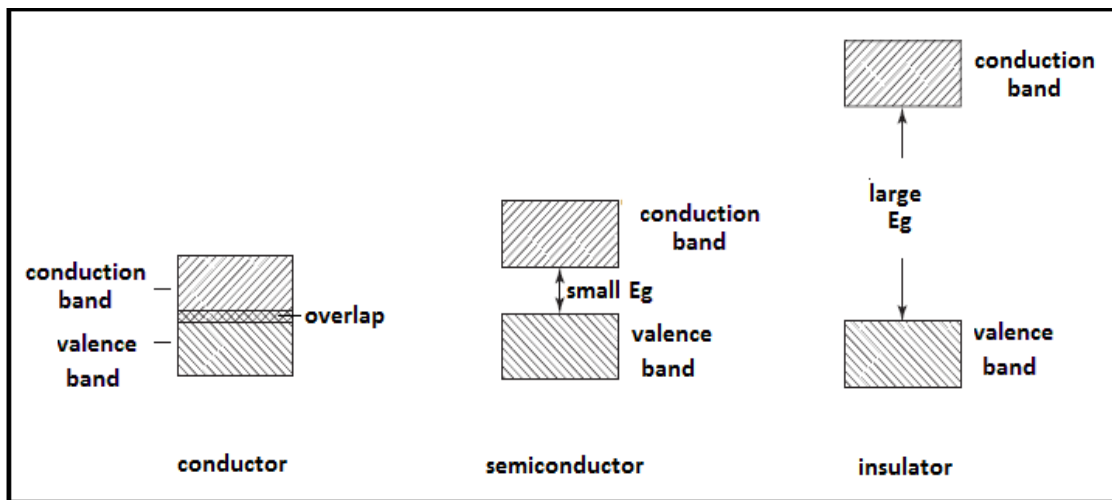


Fig 2.7 :The conduction and the valence bands in conductor, semiconductor and insulator.

It is clear from figure (2.7) that in conductors the valance and he conduction band are overlapping, this means that the conductivity of the conductors is very large. This is because all the valance electrons can rise to the conduction band then contribute in the electrical conductivity even at

very low temperatures. For insulator case, the energy gap is very wide, and for this reason valance electrons won't be able to jump to the conduction band, so the conduction is impossible in this material. In semiconductors the energy gap is small that even at the room temperature any valance electron can absorb amount of energy equals the value of the energy gap, and liberates from its band to the conduction one with a potential energy equals to the energy gap. But if the electron acquires more than the energy gap, then it has a potential ($P.E$) and a kinetic energy ($K.E$) as follows [73-75],

$$E = P.E + K.E = E_g + \frac{k^2}{2m_e^*} \quad (2.66)$$

Where E is the electron energy k is the momentum , and m_e^* is the effective mass of the electron.

When electrons liberate the valance band they leave holes, where these holes can also participate in the electrical conduction as shown in figure (2.8). Conductivity of semiconductors can be easily increased as the provided energy increases or if doped with special atoms [75].

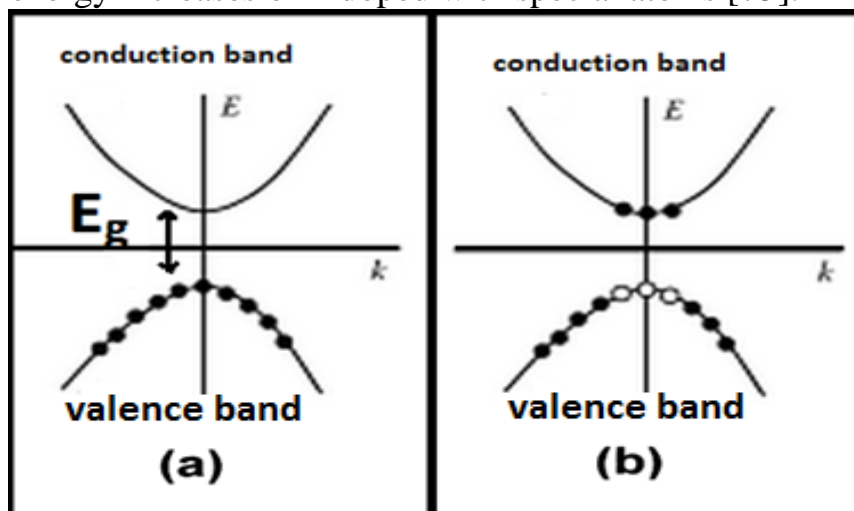


Fig 2.8: (a) Electrons (solid dots) occupy the (V.B) (b) electrons leave holes in (V.B) when they travel from to (C.B)

2.2.2 The Absorption of the Light in the Matter

The quantitative measure of how a material absorbs the light is given by its absorption coefficient (α) [76]. α and n together are usually used in the optical behavior of the solid crystals characterization [77]. The absorption coefficient (α) can be determined more accurately through using the transmittance and reflectance spectra for films which are grown onto glass substances [78],

$$T = (1 - R_{glass})(1 - R_{film})e^{-\alpha \cdot d} \quad (2.67)$$

However for transparent films. The reflection coefficient values for films and glass are very small (less than 5%) thus [58],

$$\alpha \approx -\frac{1}{d} \ln(T) \quad (2.68)$$

Where $T = \frac{I_x}{I_0}$, which is the transparency spectra and d is the sample thickness

Alternatively, one may get use from the fact that, $T+R+A = 100\%$, where $A = \alpha \cdot d$ is the total absorbance in the films. This type of analysis considers only the light dynamics between the air and film and doesn't consider the back scattered beam from glass [78]

In semiconductor a known process called "optical absorption" occurs if an electron in the valence band absorbs energy from an incident photon, and as a result transforms to the conduction band, there are two possible transitions [79]:

1- Direct transitions.

2- Indirect transitions.

The first one results if the bottom of the conduction band lies directly above the top of the valence band. If the bottom of the conduction band does not lie above the top of the valence band, then the second transition may occur, figure (2.9). So, direct transition needs a direct transition of electrons from the valence band to the conduction band, so there is no change in the momentum of the electrons thus the energy is conserved as shown in Figure 2.9 (a). Hence a wave vector k for electron remains unchanged in E-K space. The optical transition is denoted by a vertical upward arrow. But a change in the crystal momentum, is involved in an indirect transition case. Since these must satisfy the momentum conservation laws. The only way such a transition can take place is through the emission or absorption of a phonon with wave vector q as [73];

$$K' \pm q = k + K$$

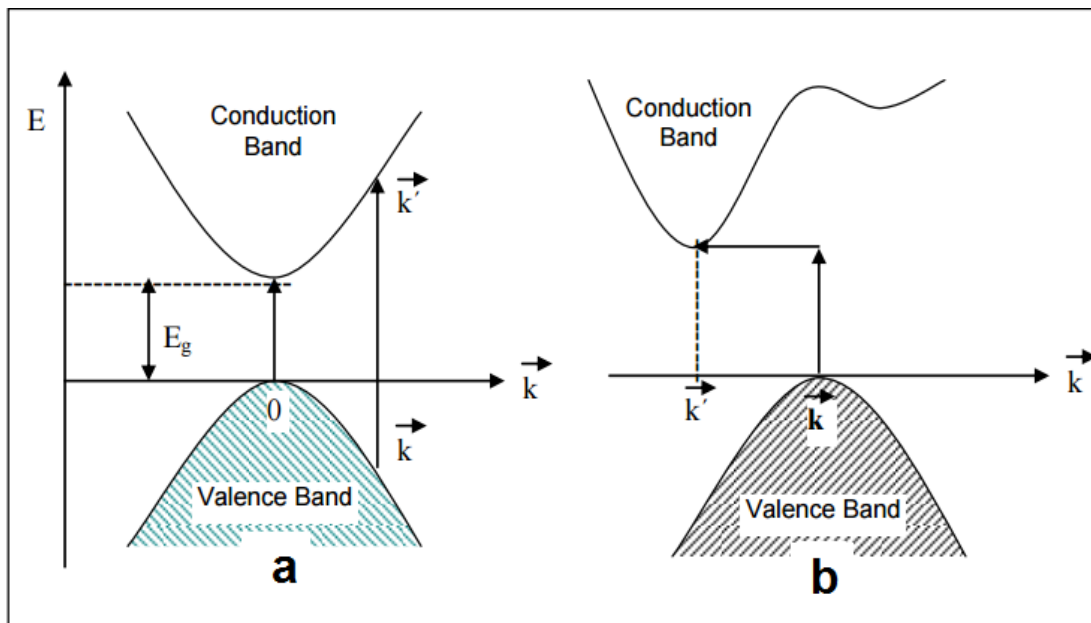


Fig 2.9 :Types of energy band gap (a) direct (b) indirect

2.2.3 Optical Band Gap measuring Technique

The measurement of the band gap of materials is important in the semiconductor, nanomaterial and solar industries. It can be found from the absorption and reflection spectra by spectroscopy, from the thermal activation energies in electrical conductivity measurement, or from photoconductivity measurement [73].

In both direct and indirect the transition may be allowed or forbidden according to the transition probability, which is independent of energy. The optical absorption coefficient (α) of a solid crystal is related to the incident photon energy near $k=0$, as the following equation [79],

$$\alpha = \frac{B(E - E_g)^p}{E} \quad (2.69)$$

where B: is constant depending on the transition probability, E_g : the band gap and p : is an index depends on the optical absorption type and takes many values like 2 , 3 , 1/2 or 3/2 for indirect allowed, indirect forbidden direct allowed, and direct forbidden transitions, respectively.

When α is plotted vis E, equation (2.69), it will be seen that at the absorption edge α rises rapidly above background, thus the energy gap can be determined by extrapolating the linear part of absorption to the value of absorption coefficient which is assumed to represent background [73, 80].

2.2.4 Dispersion

As we said, refractive index is one of the most useful optical parameters of a material, which depends on the wavelength of the electromagnetic wave by a popular dispersion relation. Dispersion is an intrinsic property of all dielectric materials [81].

The complex refractive index, equation (2.19), can be related to the complex dielectric permittivity equation (2.20), as follows [58,72],

$$n^* = n - ki = \sqrt{\varepsilon_r - i\acute{\varepsilon}_r} \quad (2.70)$$

This is called the dispersion equation, which means that the of the light beam passes through a dielectric material it will be exposed to attenuation and dispersion. Equation (2.68) gives,

$$n^2 - k^2 - i2nk = \varepsilon_r - i\acute{\varepsilon}_r \quad (2.71)$$

So,

$$n^2 - k^2 = \varepsilon_r \quad \text{and} \quad 2nk = \acute{\varepsilon}_r \quad (2.72)$$

From equation (2.71) n and k can be written in terms of ε_r and $\acute{\varepsilon}_r$ according to,

$$n = \sqrt{\frac{1}{2}\varepsilon_r \sqrt{1 + \left(\frac{\acute{\varepsilon}_r}{\varepsilon_r}\right)^2} + \frac{\varepsilon_r}{2}} \quad (2.73)$$

$$k = \sqrt{\frac{1}{2}\varepsilon_r \sqrt{1 + \left(\frac{\acute{\varepsilon}_r}{\varepsilon_r}\right)^2} - \frac{\varepsilon_r}{2}} \quad (2.74)$$

We can find both n and K by measuring the reflectance of a material as a function of polarization and the angle of incidence. For normal the reflectance R can be determine as,

$$R = |r|^2 = \left| \frac{1 - n^*}{1 + n^*} \right|^2 = \frac{|(1 - n)^2 + K^2|}{|(1 + n)^2 + K^2|} \quad (2.75)$$

For example, for a range of wavelengths if K is large, then the reflectance is almost unity, in this case the light will be reflected and any light enters the medium will be highly attenuated.

Explaining the dependence of electronic polarization with the frequency based on a single-oscillator model. The dielectric solid can be considered as assembly of oscillators (each atom or molecule is an oscillator), so when a dielectric solid exposed to the electric-field vector of the incident electromagnetic wave of radiation it will forcefully induce the dipole oscillations in the material, i.e, it displaces the electron shells to vibrate from their equilibrium positions about the positive nucleus with a single resonant frequency ω_0 , giving rise to polarization. Thus, the motion of an electron (or an ion) can be described as a harmonic oscillator one by the following equation [82],

$$m \frac{d^2x}{dt^2} + mG \frac{dx}{dt} + m\omega_0^2 x = qE_x \exp(i\omega t) \quad (2.76)$$

Where the solution of this equation will be,

$$x(t) = \frac{qE(x, t)}{m[(\omega^2 - \omega_0^2) + iG\omega]} \quad (2.77)$$

Where m is electron's mass, ω_0 is the natural frequency of the oscillator G is the damping factor and $E(x, t) = E_0 \exp(i\omega t)$ is the electric field in the x direction.

The induced dipole moment is,

$$p = -q x(t) = \text{Real}\left[\frac{q^2 E(x, t)}{m[(\omega^2 - \omega_0^2) + iG\omega]}\right] \quad (2.78)$$

In a static electric field case the induced dipole moment is proportional to the applied electric field as follows,

$$p = \text{Real}[\alpha_e E] \quad (2.79)$$

Where α_e is the electronic polarizability.

By comparing (2.78) with (2.79) we can say that,

$$\alpha_e^* = \frac{q^2}{m[(\omega^2 - \omega_0^2) + iG\omega]} \quad (2.80)$$

Which can be written in this $\alpha_e^* = \alpha_e - i\alpha_e'$ form as,

$$\alpha_e^* = \frac{q^2}{m} \left[\frac{(\omega_0^2 - \omega^2)}{[(\omega_0^2 - \omega^2)^2 + iG^2\omega^2]} - \frac{G\omega}{[(\omega_0^2 - \omega^2)^2 + iG^2\omega^2]} i \right] \quad (2.81)$$

$$p(t) = \text{Real}[N(\alpha_e - i\alpha_e')E_0(\cos\omega t + i\sin\omega t)] \quad (2.82)$$

Where N is = the number of atoms / unit volume .

$$p(t) = N\alpha_e E_0 \cos\omega t + N\alpha_e' E_0 \sin\omega t \quad (2.83)$$

$$p(t) = \frac{Nq^2}{m} \left[\frac{(\omega_0^2 - \omega^2)E_0 \cos\omega t}{[(\omega_0^2 - \omega^2)^2 + G^2\omega^2]} + \frac{G\omega E_0 \sin\omega t}{[(\omega_0^2 - \omega^2) + G^2\omega^2]} \right] \quad (2.84)$$

Where the first term of polarization is in phase with the applied electric field p-polarization and the second term lags 90° with the electric field s-polarization. Now Equation (2.77) can be written in terms of dielectric constant that,

$$p(t) = \text{Real}[\varepsilon_0(\varepsilon^* - 1)E_0(\cos\omega t + i\sin\omega t)] \quad (2.85)$$

So,

$$\varepsilon_0(\varepsilon_r^* - 1) = N\alpha_e^* \quad (2.86)$$

Substitute α_e^* from equation (2.80) in the above one we have,

$$\varepsilon_r^* = 1 + \frac{Nq^2}{\varepsilon_0 m[(\omega^2 - \omega_0^2) + iG\omega]} \quad (2.87)$$

Thus,

$$\varepsilon_r = 1 + \frac{Nq^2(\omega^2 - \omega_0^2)}{\varepsilon_0 m[(\omega^2 - \omega_0^2) + G^2\omega^2]} \quad (2.88)$$

$$\varepsilon_r' = 1 + \frac{Nq^2\omega G}{\varepsilon_0 m[(\omega^2 - \omega_0^2)^2 + G^2\omega^2]} \quad (2.89)$$

These equations indicate that in the neighborhood of $\omega = \omega_0$ the real part is zero and the imaginary one has maximum value, this means that there is an absorption maximum and that n increases rapidly on decreasing ω through this region. With continuing decrease in ω , n will pass a maximum and then fall asymptotically as ω goes further away from ω_0 [83].

As $\omega \rightarrow 0$, ε_r and hence k also approaches zero and n becomes,

$$n = \sqrt{1 + \frac{Nq^2}{m\varepsilon_0\omega_0^2}} \quad (2.90)$$

This is the undispersed refractive index, generally referred to as the refractive index of a material for $\omega \ll \omega_0$; n_0^2 is also referred to as the high-frequency dielectric constant. However, in general n_0 is different from the static or low frequency (or nonoptical) dielectric constant.

Consider a plane-polarized light beam propagates in the z direction passing through a material. According to equations (2.15) and (2.19) the velocity of the light wave inside the material will be,

$$\frac{1}{v} = \frac{n}{c} - i \frac{k}{c} \quad (2.91)$$

The electric field of the propagate wave can be written as a function of the displacement, z , and time t , as follows [82],

$$\begin{aligned} E(z, t) &= E_0 \exp \left[i\omega \left(t - \frac{z}{v} \right) \right] \\ &= E_0 \exp \left[i\omega \left(t - \frac{nz}{c} \right) \right] \exp \left(-\frac{\omega kz}{c} \right) \end{aligned} \quad (2.92)$$

Where ω is the angular velocity of that electromagnetic wave, and the term $\exp \left(-\frac{\omega kz}{c} \right)$ is called the damping factor, representing the attenuation of the amplitude of $E(z, t)$ with z due to the absorption of the electromagnetic energy of the light wave by the material. Thus, the light intensity at point z can be determined by the following relation:

$$\frac{I(z)}{I_0} = \frac{E^2(z)}{E_0^2} = \exp \left(-\frac{2\omega kz}{c} \right) \quad (2.93)$$

Look to equation (2.68), it is clear that the absorption coefficient can be expressed in terms of wavelength as,

$$\alpha = \frac{2\omega k}{c} = \frac{4\pi k}{\lambda} \quad (2.94)$$

2.3 Deposition techniques of WO₃-based thin films

The investigation on film materials become the most important in the last few years, because of its variable applications in the fields of electrics and electronics, thermotics, optics, and others as in the previous studies that we mentioned in Ch.1, so we can say that without the development of film materials many great developments and inventions in many areas could not be found, for that reason many coating techniques were developed. In this section we will show some of these methods that have been used in WO₃ films preparation.

In general one can classify all coating techniques into 5 major groups (each group includes many different techniques) as follows [84]:

- 1-physical vapor deposition (PVD).
- 2-Chemical vapor deposition (CVD).
- 3-Liquid absorption coating.
- 4-Thermal spray.
- 5-Mechanical coating.

The discussion of all these ways and their kinds and displaying their applications requires a great time, so we here discuss the common deposition methods of WO₃ thin films, such as sputtering, vacuum evaporation, spin coating, dip coating, sol gel method.

2.3.1 Sputtering deposition:

It is a widely used technique, because it is easy to deposit alloys, it produces good coverage and its small radiation damage. The basic process, look to figure (2.10), is as follows [85,86]:

- 1- A target(cathode), or source of the material desired to be deposited, is fired with energetic gaseous ions accelerated from a plasma, typically lazy gas ions , such as Argon (Ar^+)
- 2- Then the forceful collision of that ions, Ar^+ , onto the target ejects target atoms into the space.
- 3- The ejected atoms then travel some distance until they reach the substrate(anode) and start to condense into a film. As more and more atoms gather on the substrate, they begin to unit to each other at the molecular level, forming a hard bound atomic layer. More layers of such atoms can be created this is will depend on the sputtering time.
- 4-

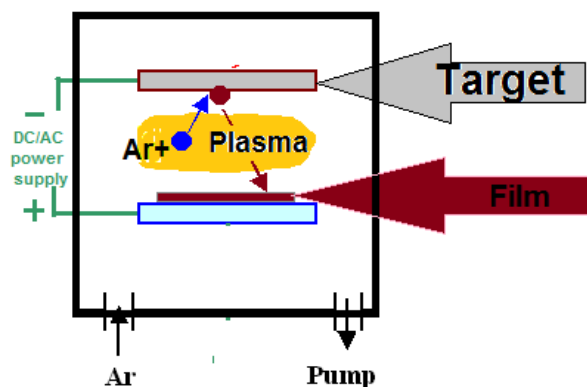


Fig 2.10 :Sputtering processes[109].

2.3.2 Spin coating techniques

Spin coating process is the predominant process in producing uniform thin films of photosensitive organic materials with (10-100) micrometer thickness [87]. It is biased on butting the deposited sol in the center of the substrate, then spin the substrate by a high speed in order to spread the deposited sol from the center towards the edge of the substrate [88]. Figure (2.8) illustrates the principles of spin coating, which can be described by four stages, deposition, spin up, spin off and evaporation which overlap with all previous stages . By using a dropper a large excess of the solution is placed onto the center of the surface of a substrate of disk-like shape this is the deposition stage, then the substrate comes into a rotation, so the solution flows over the entire surface of the disk, this is called spin up stage, and by increasing the rotational speed to typically 5000 rotation per minute (rpm), in the spin off stage the excess of liquid spins and flies off to the edge of the spinning disk due to the centrifugal force. The spinning must continue until most of the solvent evaporates in order to produce a thin film which is finally dried at 100-200 °C by convection oven or hot plate [87,89].

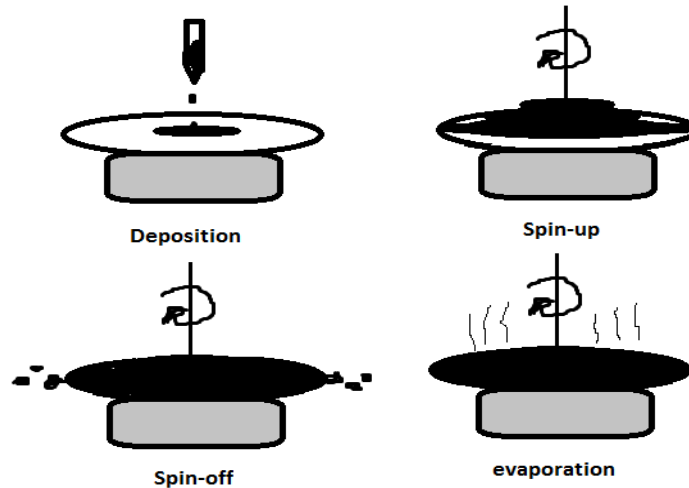


Fig 2.11 :spin coating stages.

2.3.3 Vacuum Evaporation

The vacuum evaporation deposition is a simple and a cheap PVD process which was first used, about 150 years ago, for metal or dielectric thin film on a semiconductor device. The system of this process includes a metal filament (evaporation source) , a sample holder located at an appropriate distance facing the filament. Bothm the sample and the source, are located in a glass bell jar (vacuum cell) [90,91]. Figure (2.12) shows the vacuum evaporating system. In a vacuum environment, of 10^{-6} torr or better, inside the cell a suitable material (the source) is placed with a heater, when the material heated to above of its melting point, atoms or molecules start to evaporate that they leave the source and travel inside the cell, as the substrate's surface is a cold surface compared with material's surface so the evaporated molecules will accumulate on the substrate [90-93].

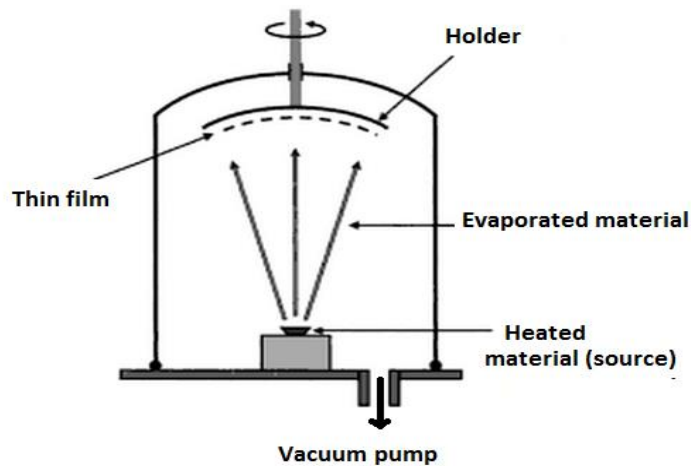


Fig 2.12 :Vacuum evaporation technique [90].

2.3.4 Sol-Gel Process

Interest in the sol-gel processing on inorganic ceramic and glass materials began as early as the mid – 1800s with Ebleman and Graham's studies on silica gels [94]. Sol differs from other solutions because the solution is a single-phase system, while sol is a colloid, a suspension of small particles of one small phase (~1-1000nm), that gravitational forces can be negligible and interactions are dominated by short-range forces. Also it differs from an aerosol which is a colloidal of particles in a gas [95]

Compared to usual thin film processes, sol-gel allows a good control of the chemical composition of the films utilizing simple equipments at low cost, especially, the heat treatment it needs low temperature because precursors can be mixed at molecular level in the solution and thus a high homogenous film can be obtained [96]. Sol gel industry would most likely to producing many more goods both in quantity and in assortment, than it produces today without these difficulties in non destructive drying [97]. There are main four steps that guide the sol-gel procedure, these are [94-98]:

- 1- Hydrolysis and polycondensation: inorganic and metal-organic raw materials are dissolved, and via condensation reactions, a colloidal suspension (sol) are produced.
- 2- Gelation: the transformation of the (sol) from a network to a continuous liquid phase (gel)
- 3- Aging: sol-gel solution which is produced either poured into a mold until transfer to gel , or it applied to a substrate by another technique such as dip coating, spin coating, spray coating, or roll coating.
- 4- Drying: by heating the gel layer will rid of any water and other volatile liquids. This process is complicated because of the fundamental changes in the structure of the gel, according to this step ceramic or glass bulk part or a thin film on a plastic, glass, ceramic or metal substrate will be resulted. This means that, differently dried gels will have different structural evolution with heat treatment.

2.3.5 Dip coating

Among the available deposition methods, dip coating is mostly wide used especially for industrial, because it is simple, low cost, high coating quality process [99]. By dip coating process it is possible to deposit thin films onto any irregular shaped object, that any substrate with any geometry can be used and this feature distinguishes the dip-coating technique[100]. Many material can be used to prepare thin films by sol-gel dip coating, But metal oxides are the most used [99]. Dip coating process designates the deposition of a wet liquid film by normal and vertical withdrawing a sample from a liquid bath at a specific speed [101]. Preparing a thin film by dip coating method involves several steps, look to figure (2.13). Starting by

immersing the substrate into a reservoir of solution for suitable time and constant velocity to ensure the completely and regular coverage of the substrate. Then withdrawing the substrate from the solution that the moving substrate pulls the liquid in a fluid mechanical boundary layer which splits in two above the bath, the outer layer back to the bath, and the remaining solvent is evaporating and draining by gravity, then heated under high temperatures resulting in a well-defined dry film [99-101].

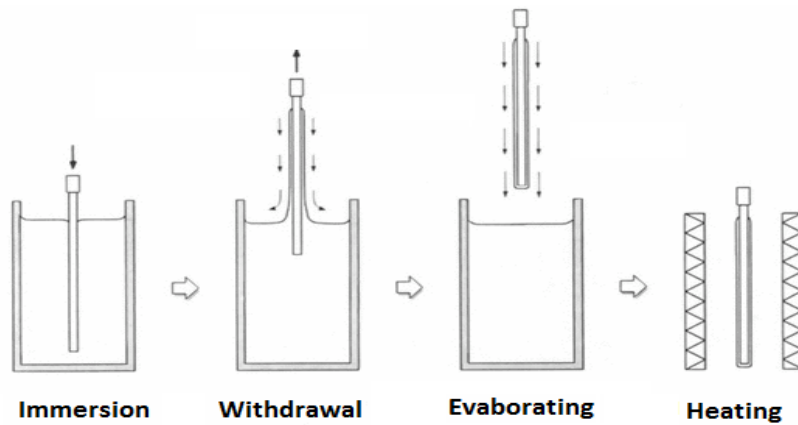


Fig 2.13: Dip coating technique steps [99].

The thickness of the resultant film (d) can be calculated by the Landau-Levich relation as follows [88],

$$d = \frac{0.94 \left((\eta U_0)^{\frac{2}{3}} \right)}{\gamma_{LV} (\rho g)^{\frac{1}{2}}} \quad (2.95)$$

Where η is the liquid viscosity.

U_0 = the speed of dipping the sample.

γ_{LV} = the liquid vapor surface tension.

ρ = the liquid density.

g = the acceleration of the gravitational force.

Chapter Three

Experimental Work

3.1 Material and film preparation

3.1.1 Chemicals and Solvents

Used materials listed below are purchased from different companies:

Tungsten Hexachloride (WCl_6) was purchased from sigma-Aldrich in (99.9%) purity. Titanium (II) Chloride ($TiCl_2$) which also was purchased from sigma-Aldrich. Commercial microscope 75mm×1 mm glass slides were taken from department of Biology at An-Najah University. Lactic glycoside ratio of 50:50 was purchased from sigma-Aldrich, Other materials like ethanol (99.85%) and peroxide H_2O_2 (4%) are self-packing locally.

3.2 Preparation of the thin films

3.2.1 Substrate Cleaning Process

Glass substrates 75mm × 13mm have been prepared to be ready for the deposition of the film. Producing pure, uniformly, and well adherent films require using pre-cleaned substrates. The following effective method for glass cleaning was employed [102-104] as in the following steps:

- 1) Cleaning with liquinox soap water to remove any dust or attachments.
- 2) Washing the soap well by deionized water.

- 3) The substrate was then dipped in dilute H_2O_2 , then dilute H_2O_2 was boiled at 75°C for 30 min to dissolve any unclean attaches.
- 4) Washing again with deinized water .
- 5) The substrates were saved in a temporarily well covered beaker filled with ethanol until the films preparation processes begin.
- 6) Before preparing the films, the substrates are extracted from ethanol and dried in an oven less than 60°C . Then they are left to cool to room temperature before preparing the films.
- 7) During all cleaning and preparation process, the substrates are always handled with care from edges (without touching the surface). Moreover, cloves are worn to prevent any dirt, cells, or even protein stuck on our hand to fall on substrate or films.

3.2.2 Preparation the WO_3 Sol-gel solution doped with Ti

Titanium (Ti) atoms were assumed to compensate Tungsten (W) atoms in the tungsten trioxide (WO_3) structure after annealing, this can be written as in the equation form " $\text{W}_{1-x} \text{Ti}_x \text{O}_3$ ".

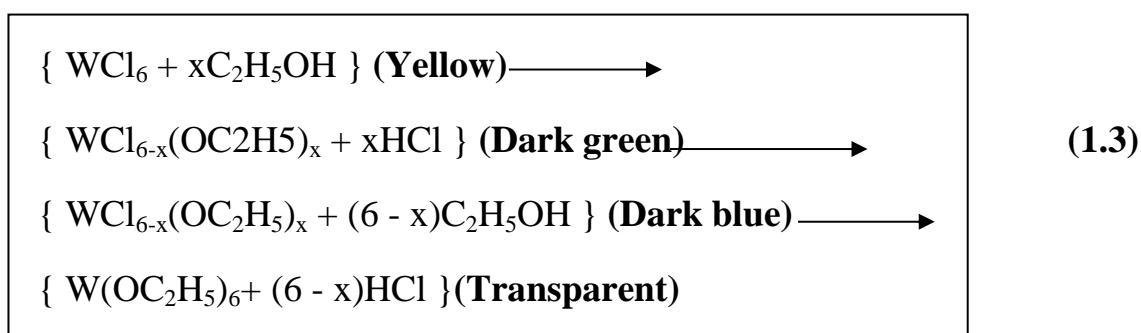
WO_3 was doped with different concentrations of Ti atoms that range from (0% to 40%) molar in steps of 10%. Preparation of dipping solution was done in accordance with literature [105-107]. Different weights of WCl_6 and TiCl_2 that correspond to different atomic concentrations are calculated and listed in Table (3.1). Then they were mixed in a rubber closed flask contains 10 mL ethanol and 1 mL glycerol, this ratio of glycerol is the most suitable ratio to obtain the optimal regular thickness .

Table. (3.1): List of intended compositions, WCl_6 and $TiCl_2$ mass used in sol-gel preparation.

Sample no.	Composition	WCl_6 (gm) $\times 10^{-2}$	$TiCl_2$ (gm) $\times 10^{-2}$
1	WO_3	174.40	0.00
2	$W_{0.90} Ti_{0.10} O_3$	157.04	5.23
3	$W_{0.80} Ti_{0.20} O_3$	139.89	10.45
4	$W_{0.70} Ti_{0.30} O_3$	122.14	15.68
5	$W_{0.60} Ti_{0.40} O_3$	104.69	20.90

The concentrations of the materials in the liquid are chosen to be 0.4 molar. This molar concentration was chosen after selection between molar concentration ranges from 0.25 M to 0.5 M in steps of 0.05 M. The mixture was then kept to react in 120 W ultrasonic vibrator which vibrates at frequency of 400 kHz in a Sonicator MRC (Model, AC-120H), Fig (3.1), for two hours. The water inside the ultrasonic vibrator was kept at constant temperature 25°C. All reaction process was done in the fume hood due to harmful gasses produced from the reaction.

At the beginning of the chemical reaction the color of the solution was yellow, after 30 mints it became dark green, and at the end of process it was dark blue. This indicates that the solution reaction undergoes a different reaction steps before its final results, this was also observed by [130], the reactions are summarized as follows:



3.2.3 Preparation the WO₃: Ti thin films by dip coating method

The prepared sol-gel solutions were deposited on the pre-cleaned glass slides by using dip coating method.

Dipping was done using a local designed and manufactured dip coater which was designed at physics department by Mr. Mohammad Bahjat and Dr. Iyad Saadeddin , it is shown in figure (3.2),

The steps of dip coating process were carried out as follows (see Fig. (3.3)) within safety regulations:

- 1- The prepared sol-gel was put in a 10.0 mL beaker and fixed vertically under the motor.
- 2- The glass substrate was coated by Adhesive tape on one side while the other still without coating. This process is done to make sure to get one thin layer on a specific side of the film.
- 3- The cleaned substrate which was coated by Adhesive tape was dipped in the prepared sol-gel with a speed of 0.65 mm/s. This very slow speed in is performed to get sufficiently thin film. In addition, the upper part of the film was not immersed to easily film holding.
- 4- The substrate left immersed in the solution for 3 min to insure good exposure and adhesive of the solution to the glass substrate.
- 5- Drawing out the film with the same speed of dipping to ensure the production of a uniform film.
- 6- The glass coated film was lifted 5 minutes above the beaker to drop any extra material and to allow drying the film.

7- Finally, grown films were immediately annealed at 160 °C, which is the most optimal temperature to reveal the maximum transparency.



Fig 3.1: ultrasonic vibrator



Fig 3.2: Local designed and manufactured dip coater designed at physics department by Mr. Mohammad Bahjat and Dr .Iyad Saadeddin.

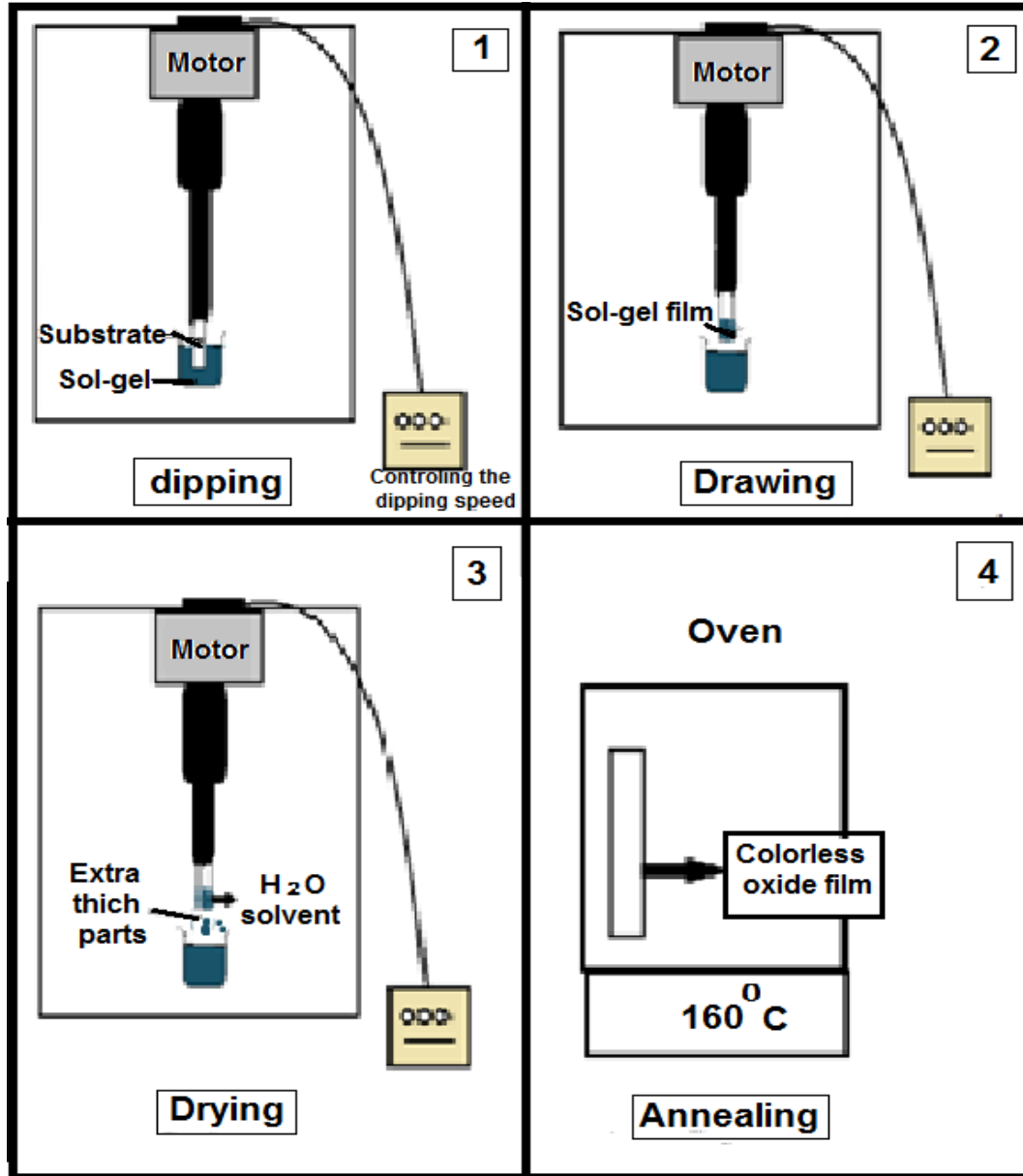


Fig 3.3: $\text{WO}_3:\text{Ti}$ thin films deposition steps.

3.3 Measurements

3.3.1. X-Ray Diffraction (XRD)

The structural analysis of all the thin films were performed with a PHYWE Series X-Ray Automatic Diffractometer with $\text{CuK}\alpha$ ($\lambda=1,54059\text{\AA}$). The diffractometer reflections were taken at room temperature and the value of 2θ were swapped between 2° and 90° . The sample was fixed in the rotating

axis of the diffractometer, then X-rays was focused on it, then the rotating axis began to rotate, the changes in the diffracted X-ray intensities at different angles were collected. The XRD patterns were recorded at Arab American University, Jenin city, Palestine . The results are to be used to determine the crystal structure of the samples by special computerized analysis methods using Excel and X-ray programs.

3.3.2. Transmittance and reflectance

The transmittance (T) and reflectance (R) spectra of all Ti doped WO_3 films were carried out at room temperature by using Evolution 300 scanning spectrophotometer in the wavelength range from 190 to 1100 nm. The spectra were recorded at Arab American University, Jenin city, Palestine. The reflectance was recorded using VEE MAX II variable angle reflectometer The substrate transmissivity (reference beam) is corrected by introducing an uncoated cleaned glass substrate in the reference beam. The results are employed for determining the thickness and the dielectric dispersion relation of the samples.

Chapter Four

Results and Discussion

In this work semiconducting electrochromic thin films of WO_3 nanoparticles, doped with different atomic concentrations of Ti, have been prepared and studied.

4.1 X-Ray diffraction (XRD):

The structural tests of all the thin films were done by XRD method. The XRD patterns for WO_3 : Ti with different Ti molar concentration (0 – 40 % in steps of 10 % each) heated under temperature of 160°C are shown in Figure (4.1). When the X-rays patterns of obtained films were plotted on the same axis of that of glass substrate, no intensive patterns were observed. The non intensive X-ray reflections indicate the amorphous nature of structure. This result is acceptable as compared with literature data which indicates the polycrystallinity about 350°C [108,109].

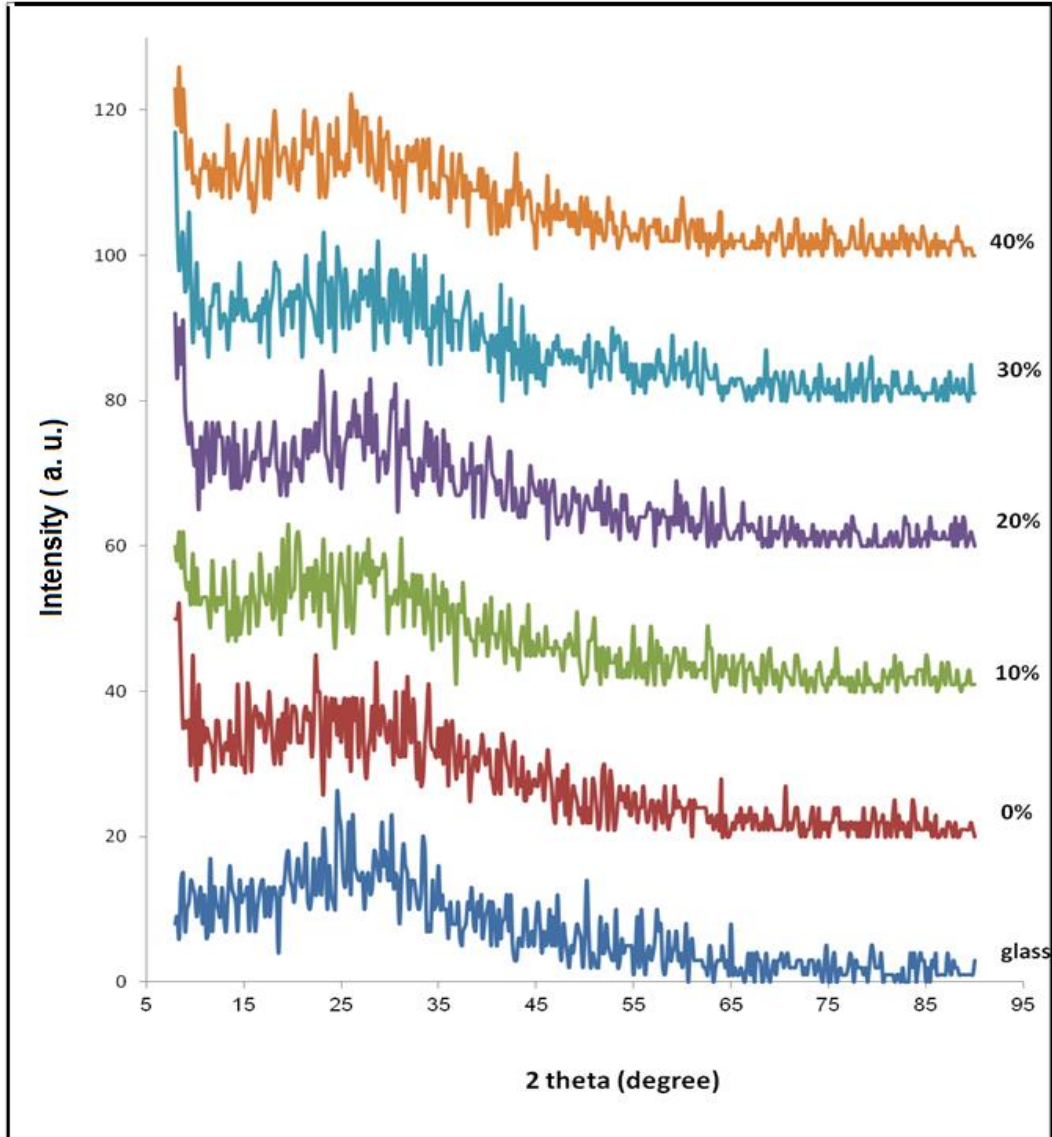


Fig 4.1: XRD patterns of Ti doped WO_3 thin films prepared at different Ti concentration with non doped WO_3 film (10%, 20%, 30% and 40%) in comparison.

4.2 The Transmission spectra (T):

A good method for investigating the band structure and energy gap (E_g) of semiconductors and of both crystalline and amorphous non-metallic materials is the analysis of optical transmission spectra.

The transmittance (T) spectra of all Ti doped WO_3 films were accomplished and presented as a function of the wavelength in figure (4.2)

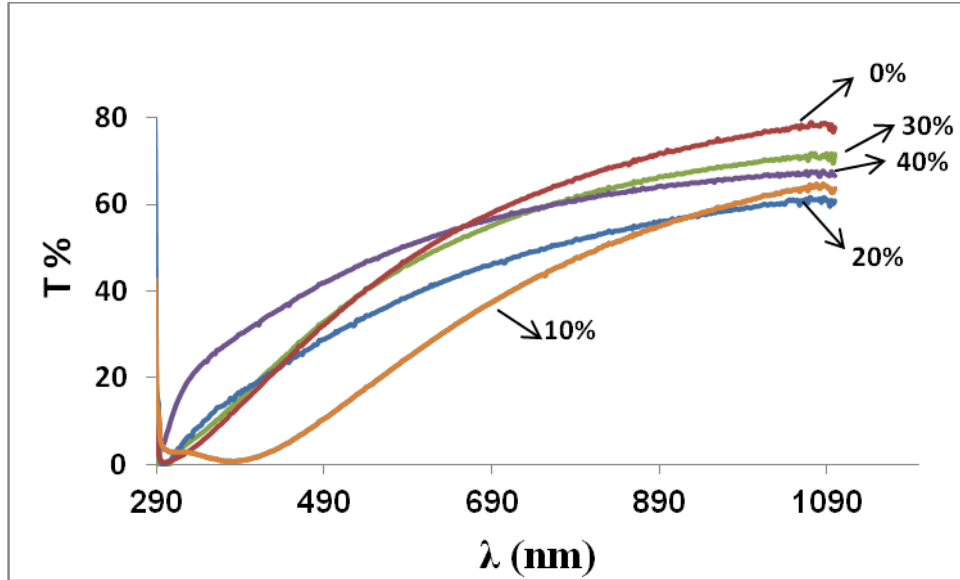


Fig 4.2: The transparency (T) data for WO_3 thin films doped with different concentrations of Ti.

All the samples show transmittance that increases with increasing incident wavelength where the maximum point of transmission is obtained for the undoped film. In addition, the transmission spectra for the doped films reflect a systematic increase of transmittance with doping concentration.

4.2.1 The absorption coefficient (α)

From the transmittance spectral data, the absorption coefficient was calculated, in order to find the band gap E_g , using (2.68) relation which discussed in chapter 2,

$$\alpha = -\frac{1}{d} \ln[T] \quad (4.1)$$

Where d: is the thickness thin film

The data are illustrated in Fig. (4.2). All WO_3 samples doped with Ti exhibited lower absorption coefficient than undoped WO_3 alone. The max absorption coefficient for undoped WO_3 has a value $8 \times 10^4 \text{ cm}^{-1}$ at

wavelength 311nm. However, for doped samples, the absorption coefficient decreases significantly with increasing Ti concentration and ranges from $(1 \times 10^3 \text{ to } 3 \times 10^4) \text{ cm}^{-1}$ at the same wavelength.

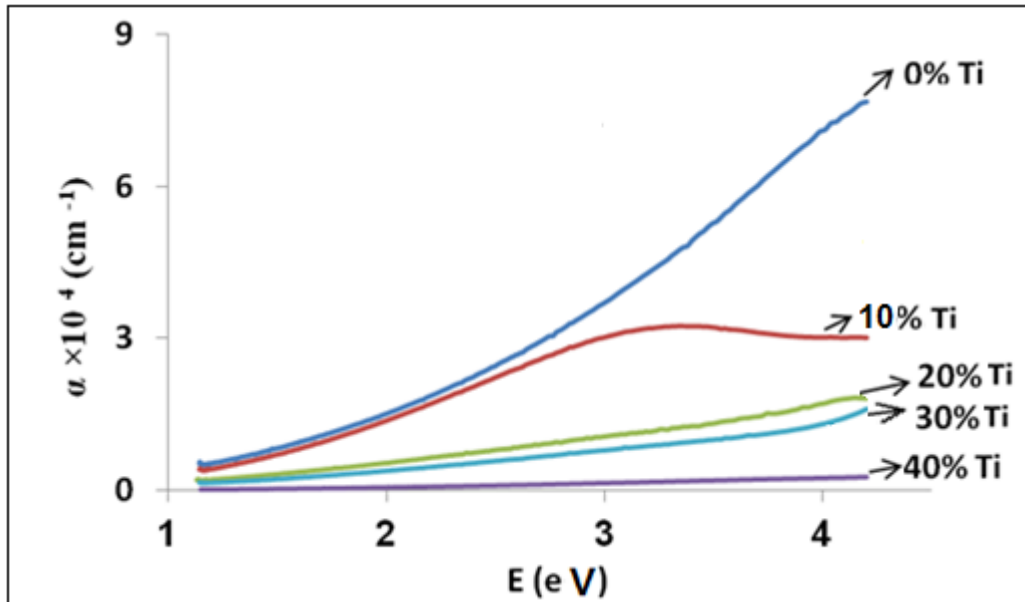


Fig 4.3: Variation of absorption coefficient as function of incident photon energy for WO_3 films doped with different concentrations of Ti .

It is also noticeable that the absorption coefficient for undoped WO_3 doesn't reach zero even at 1.0 e.V. Such behavior is an indication of the existence of energy band tails in the films that cause inter band transitions. The increase in the doping concentration of Ti decreased the inter band transitions effect. The sharp decrease in the absorption coefficient near 1.0 e.V is the main indicator for the later result.

4.2.2 The Optical Energy band gap (E_g)

In the sharp absorption region ($> 10^3 \text{ cm}^{-1}$), α can be represented by the relation (2.69) ,

$$\alpha = \frac{B(E - E_g)^p}{E} \quad (4.2)$$

where B is a constant that depends on the transition probability.

From the previous relation (4.4) it is possible to find the energy gap for the sample under investigation by plotting $(\alpha E)^{1/p}$ versus photon energy, E, at all theoretical values of p, the figures of $(\alpha E)^{1/2}$, $(\alpha E)^2$, $(\alpha E)^{1/3}$ and $(\alpha E)^{2/3}$ as function of E are illustrated in Fig. (4.8) (a), (b), (c) and (d), respectively. As a example, we show such plots for the WO₃ sample doped with 10 % Ti. All the other samples show similar behavior. It has been observed that the plots of $(\alpha E)^{1/p}$ vs E are liner over a large domain of photon energies indicating the direct allowed electronic transitions in the energy band gap. The invalidity of other electronic transitions which appear in (a), (c) and (d) are understood from the negative E-axis crossing of $(\alpha E)^{1/p}$ - E trends.

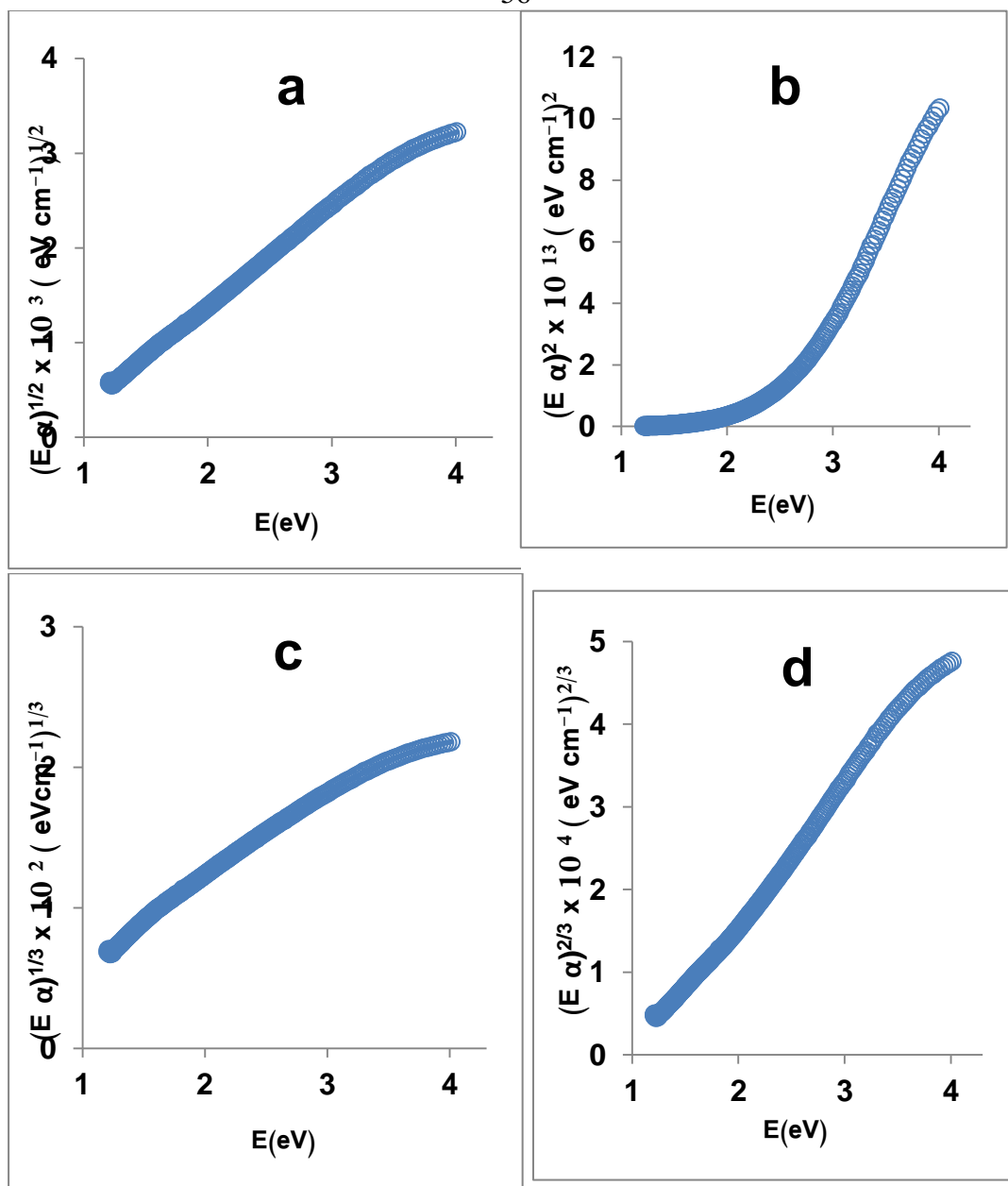


Fig 4.4: Plots of $(\alpha E)^{1/p}$ as function of E for p values being 2 (a), 1/2 (b), 3 (c) and 3/2 (d) for WO_3 thin films doped with 10% Ti .

The optical energy band gaps for all the prepared WO_3 films were measured by the extrapolation of the linear part of the curves to the energy axis, as shown in figures (4.5) and (4.6), where the intercepts will be the optical energy gaps. The measured band gaps for all the samples are listed in Table(4.1).

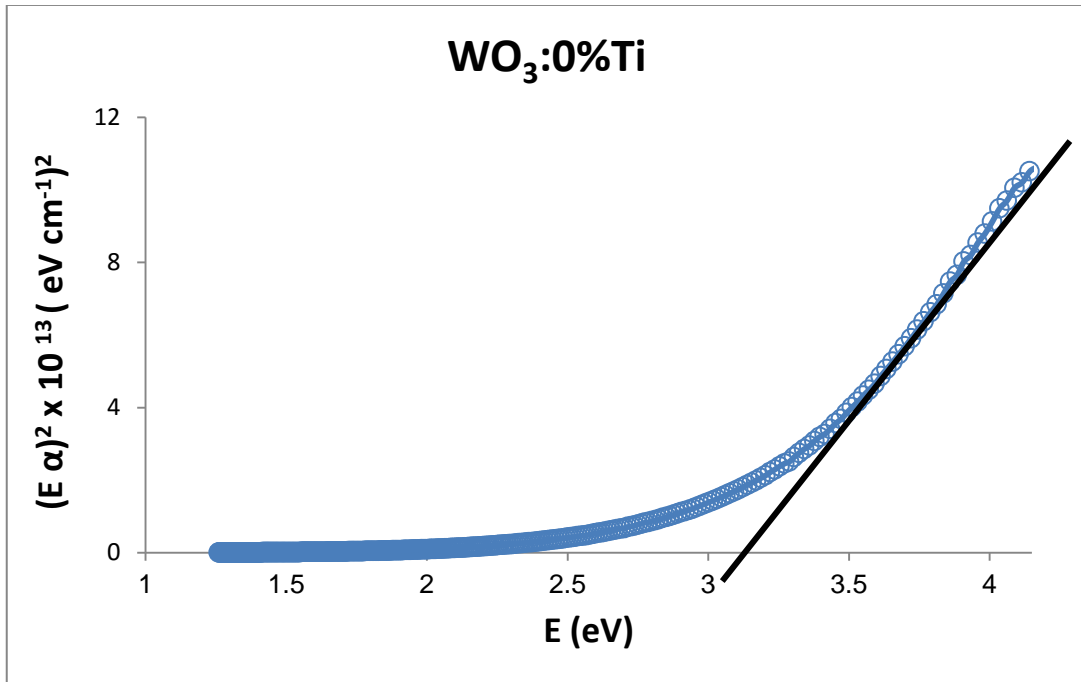


Fig 4.5: The plot of $(\alpha E)^2$ as function of E for (Ti non-doped) WO₃ thin film.

From figure (4.5) it was found that the energy gap of WO₃ is 3.1 eV. This result is very near to that founded by Rao et. al. [110].

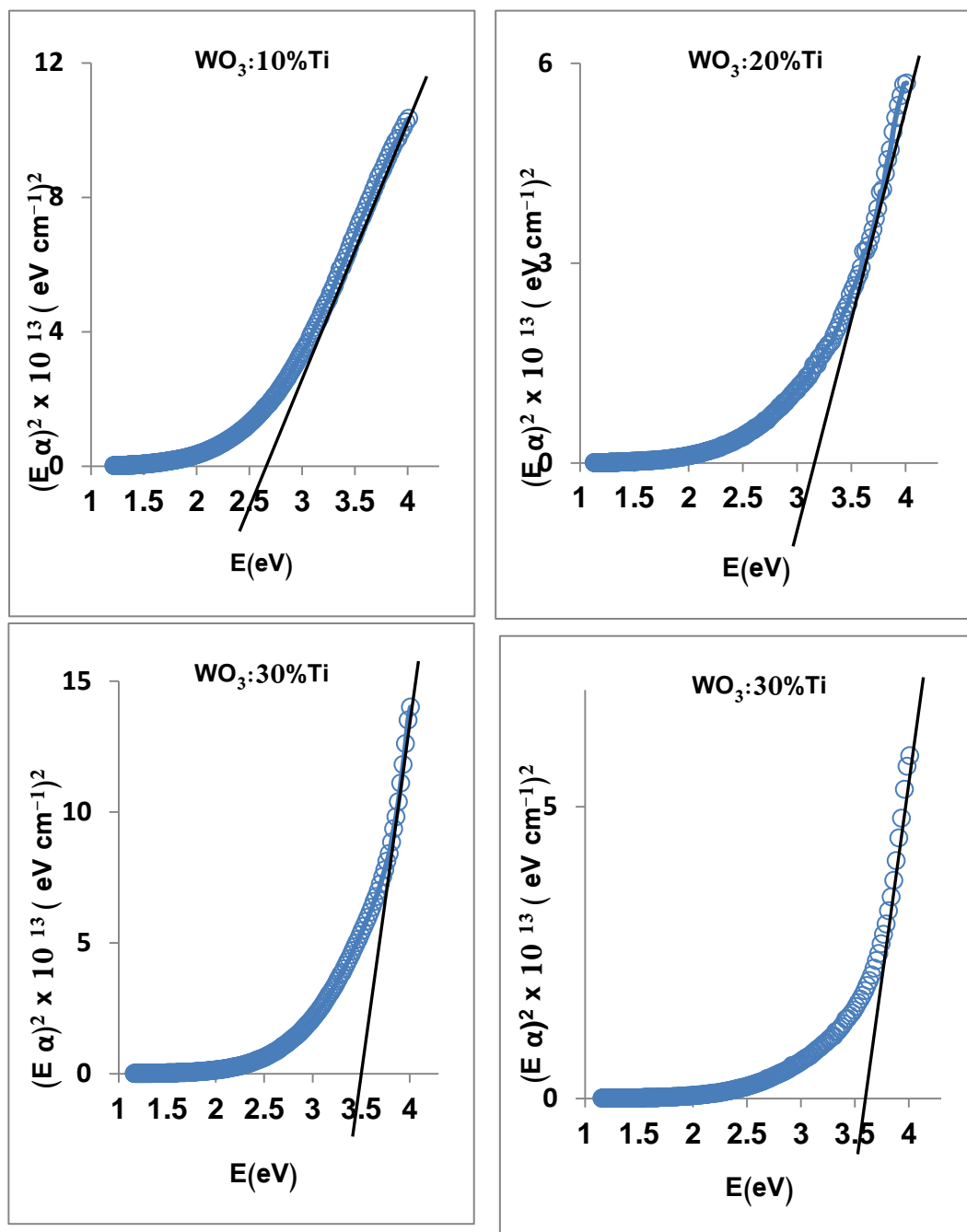


Fig 4.6: The plot of $(\alpha E)^2$ as function of E for $\text{WO}_3:\text{Ti}$ doped thin films at different concentrations of Ti.

Table 4.1 : The optical energy band gap values of doped WO₃:Ti thin film at different concentrations of Ti.

Concentration of Ti (%).	E _g (eV)
0	3.10
0.1	2.58
0.20	3.2
0.30	3.5
0.40	3.6

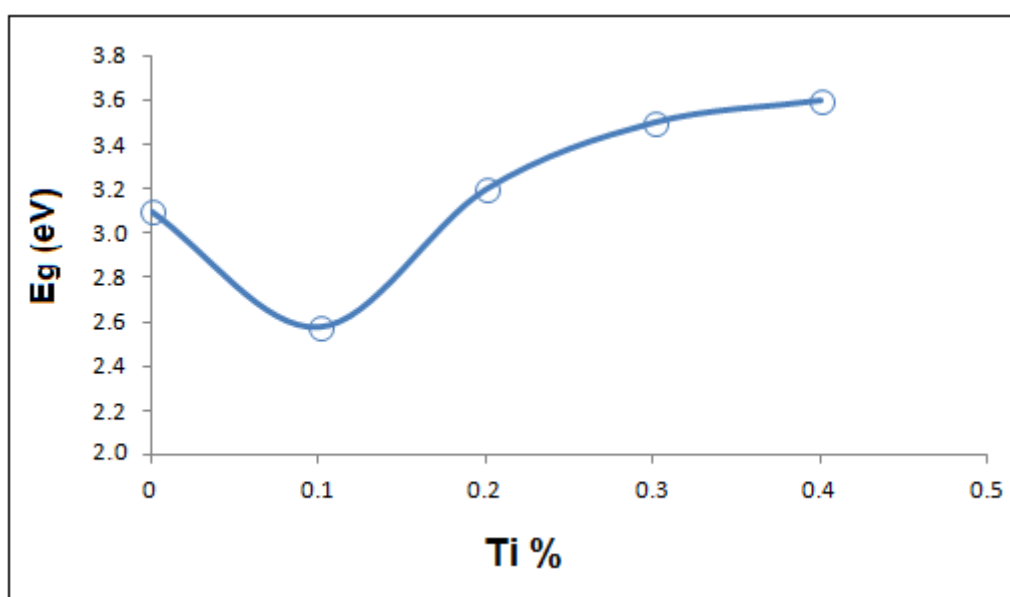


Fig 4.7: The variation of the energy gap of WO₃ thin films doped with different Ti concentration and undoped.

The electronic band structure of titanium oxide clusters were studied by H. wu and L. S. Wang [111]. The analysis of the photo electron spectroscopy for the vibratory resolved spectra for TiO⁻ and TiO₂⁻ revealed six electronic states for TiO, five of them are excited by the multi electron transitions in the photo detachment process. The TiO₂ phase have closed shells with highest occupied molecular orbital (Homo), lowest unoccupied molecular orbital (Lumo) difference of 2 e.V . The larger (TiO₂) clusters are all closed

shells with Homo- Lumo gap similar to TiO_2 with increasing electron affinities for $n=2$, 2.1 eV, for $n=3$, 2.9 eV and 3.3 eV for $n=4$. On the other hand, the photo detachment studied of WO_3 has shown that the electronic affinity for the WO_3 is 3.3 eV [112]. Since the electron affinity determines the position of the bottom of the conduction band from the vacuum level. The large decrease in energy gap upon insertion of Ti 10% indicates that the dominant transitions are between Ti and O atoms, and because the electron affinity of TiO_2 is 2.1 eV, the conduction band difference $\Delta E = 3.3 - 3.1 = 1.2$ eV, for 10% Ti is, $3.3 - 2.9 = 0.4$, $3.3 - 3.1 = 0.2$, when Ti concentration is increased more (TiO_2) n clusters increase in the film leading to a wide gap. Consistently, from the valence band orbitals point of view, the Ti atoms replace W atoms and since the electronic configuration of TiO : $3d^2 4s^2$ and for tungsten" $4f^{14} 5d^5 6s^2$, the electronic transition in WO_3 originates from O ($2p^4$) to W ($5d^5$) and for TiO_2 from O ($2p^4$) to Ti ($3d^2$). The energy difference between $2p^4$ and $5d^5$ states is larger than $2p^4$ and $3d^2$ orbitals, this explains the reason for larger energy gap of WO_3 than TiO_2 . It is also may happen that electronic transition from W($5d^5$) to Ti ($3d^2$) become more preferable at some particular concentrations.

4.3 The Reflectance (R)

A method for probing the dielectric constant (ϵ), the refractive index $n(E)$ and the thickness of thin films of semiconductors and of both crystalline and amorphous non-metallic materials is the analysis of optical reflectance spectra.

The reflectance (R) spectra of all Ti doped WO_3 thin films were carried out and plotted as a function of the wavelength as shown in figure (4.8) respectively.

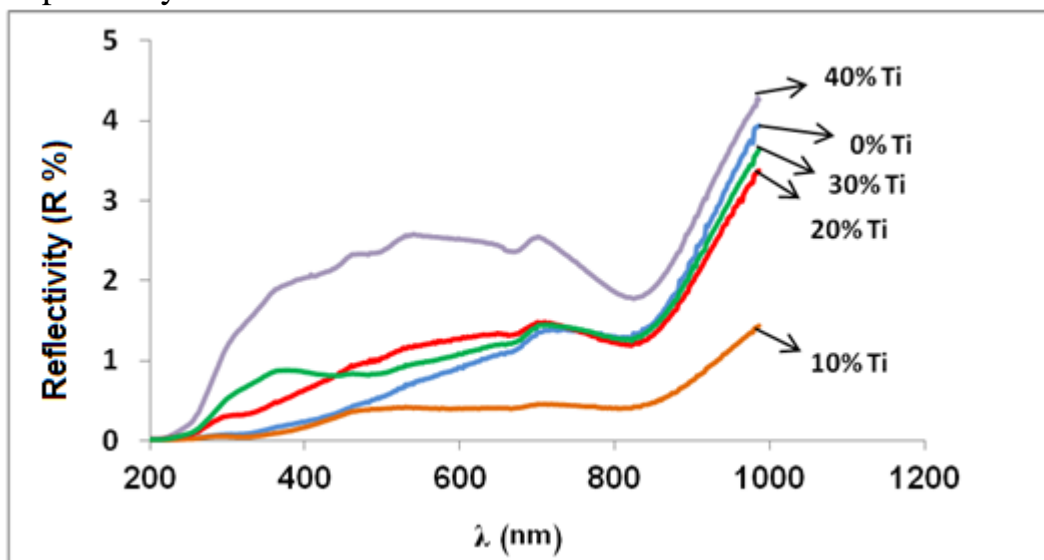


Fig 4.8: The reflectance (R) spectra for WO_3 doped with Ti at different concentrations.

For different of deferent Ti concentrations, the reflectivity measurements shows a weak reflectivity ranges from (0-3%) in the UV-visible range. However, the reflectivity begins to increase (but still in weak ranges from (2-2.5%) in the near – infra-red region ($\lambda \geq 800$ nm). Moreover the same curvature was observed in reflectivity, figure (4.9), as observed in E_g which is due to the same reason we talked about previous.

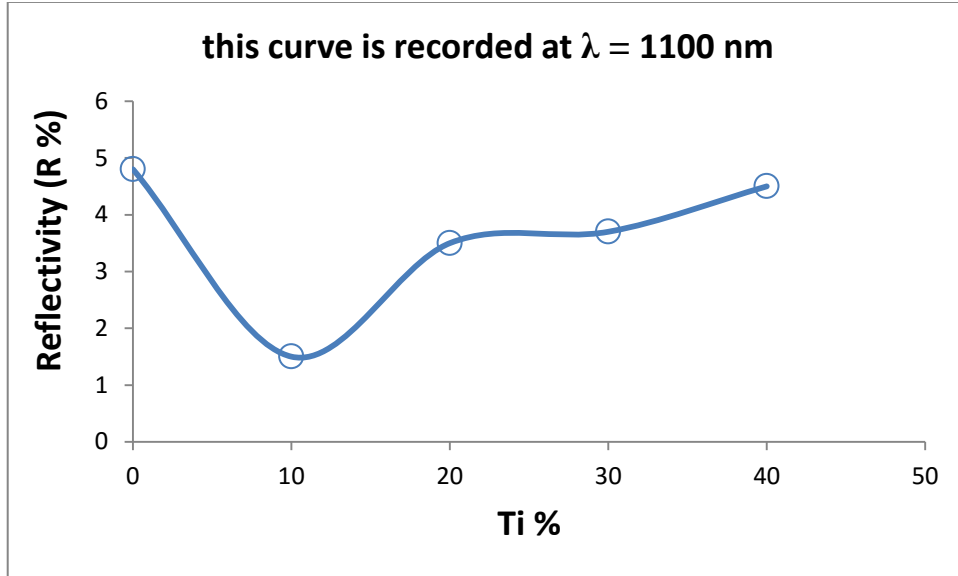


Fig 4.9: The variation of reflectivity of WO_3 thin films doped with Ti as a function of Ti concentration.

4.3.1 The dielectric constant (ϵ) :

The dielectric constant is calculated from equation (2.64),

$$\epsilon = \left(4 + \frac{\sqrt{\left(16 - 4 \left(\frac{Rs - 1}{Rs + 1} \right)^2 \right)}}{\left(\frac{Rs - 1}{Rs + 1} \right)^2} \right) \quad (4.3)$$

To understand the effect of doping Ti on the dielectric constant, the variation of the dielectric constant of WO_3 thin film, doped with different concentrations of Ti was calculated and arranged at specific wavelengths, Table (4.2). The relation between the dielectric constant and the Ti concentration was plotted at certain wavelengths as in figure (4.6). It is clear that the dielectric properties are increasing as Ti concentration increases, this is due to increasing the amount of insulating TiO_2 as the Ti

concentration increases. Hence, it is normal that the dielectric constant is increasing as the wavelength increases.

Table 4.2: Variation of the dielectric constant of WO₃ thin film, doped with different concentrations of Ti at specific wavelengths.

Ti (%)	$\lambda = 300$ (nm)	$\lambda = 400$ (nm)	$\lambda = 600$ (nm)	$\lambda = 900$ (nm)	$\lambda = 1000$ (nm)	$\lambda = 1100$ (nm)
0.00	7.51	7.61	8.06	8.99	10.41	11.33
0.10	7.49	7.57	7.72	7.96	8.49	8.98
0.20	7.66	7.87	8.30	8.79	9.95	10.66
0.30	7.80	8.02	8.17	8.90	10.15	11.00
0.40	8.24	8.82	9.17	9.29	10.63	11.49

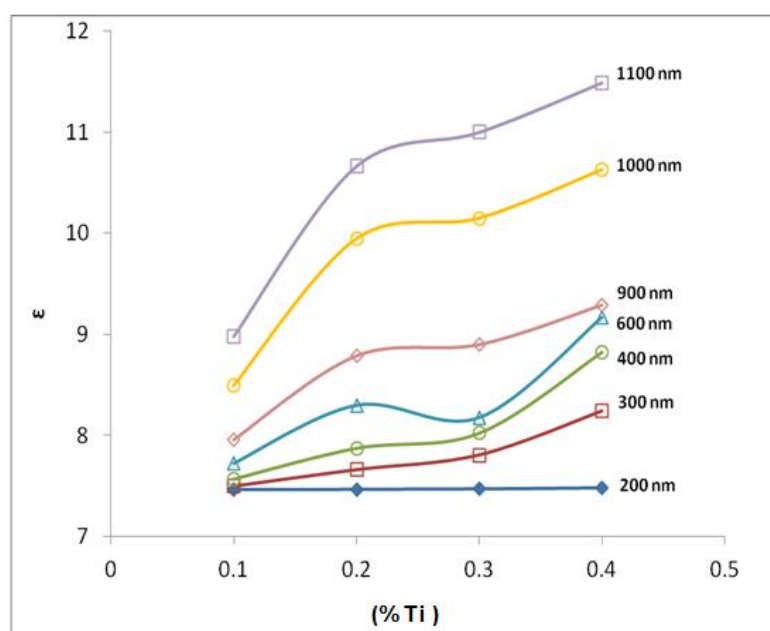


Fig 4.10: The relation between dielectric constant of WO₃ :Ti doped thin film with the concentration of Ti at certain wavelengths. .

It can be seen that the dielectric constant of WO₃ thin films increases with Ti concentration increase, this means the increase in degree of atomic polarizations, this happens as a result of electronic transfer between the 4d and 5d states and up states .

4.3.2 The thicknesses of investigated films.

The reflectance spectrums for the WO_3 thin films doped with different atomic concentrations of Ti were used to determine the film thickness of those thin films. When the light strikes a thin film both the top and bottom surfaces of the film reflect light, so the total amount of reflected light dependent upon the sum of these two reflections. Furthermore, due to the wave-like nature of light, according to the phase of these two reflections may destructively or constructively add to each other. The fringes which will appear in the resulting interference form can be used in the film thickness determination using the following expression [78]:

$$d = \frac{m}{2D_n \sqrt{(n^2 - \sin^2 \theta)}} \quad (4.4)$$

where

d = film thickness

m = number of fringes in wavenumber region used

n = refractive index

θ = angle of incidence.

D_n = wavenumber region used ($\frac{1}{\lambda_1} - \frac{1}{\lambda_2}$; cm^{-1})

Where the absolute reflectance spectra were acquired over the range ($\lambda_1 = 450 - \lambda_2 = 800$) nm.

For example the reflectance spectrum for WO_3 doped with 10% Ti has 3 fringes as shown in figure (4.11). According to equation (4.4) and in the wavelength range (450 – 800) nm the average thickness of this film was

calculated to be $0.574 \mu\text{m}$. The same thing was done for each prepared thin film in order to find the thickness of all our films as shown in Table (4.3)

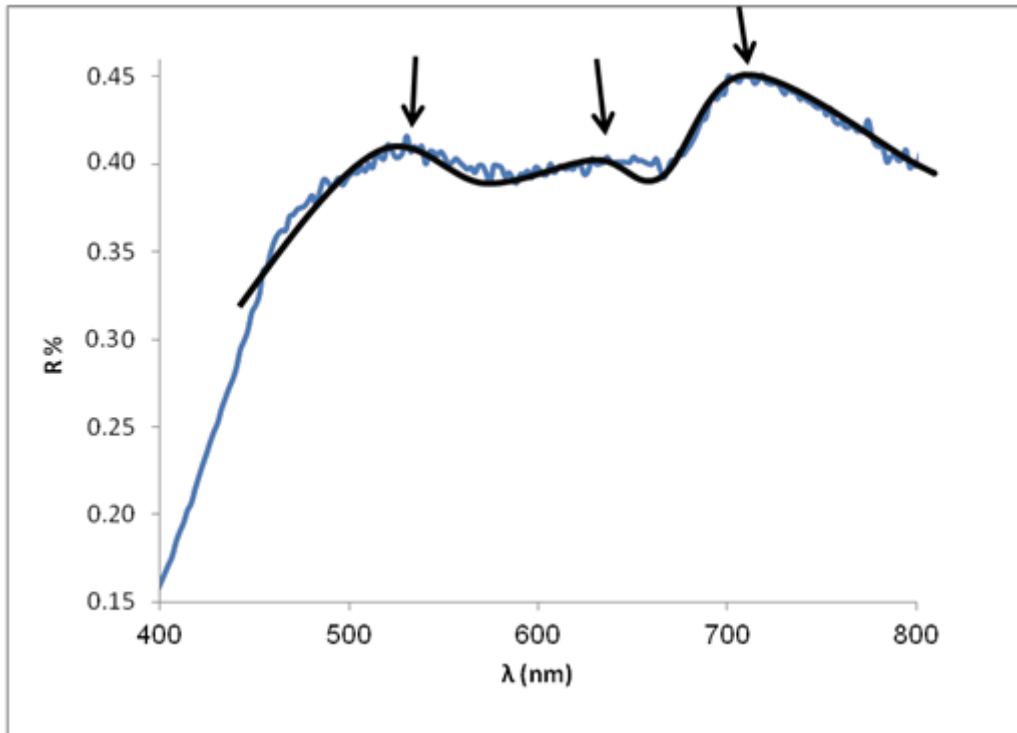


Fig 4.11: The reflectance (R) spectra for WO_3 doped with 10 % Ti .

Table 4.3 : The calculated thickness of WO_3 thin film doped with Ti at different concentration of Ti

Ti concentration (%Ti)	Thickness (μm)
0	0.373
10	0.574
20	0.757
30	0.741
40	0.703

It is clear that the thickness WO_3 thin film is increasing as Ti concentration increases to a slightly constant value, see relation (2.89). The thickness 'd' proportional to the liquid viscosity and this factor is increasing as the increasing as the Ti concentration increase.

4.4 The oscillator parameters:

The dispersive refractive index data in $E < E_g$ range may be analyzed using the single oscillator model that suggested by Wemple and DiDomenico [113]. According to the model the relation between the refractive index n^2 (E) and the photon energy E could be described as,

$$n(E)^2 = 1 + \frac{E_d E_0}{E_0^2 - E^2} \quad (4.5)$$

Where E_d and E_0 : the dispersion energy and the oscillator energy respectively, the first one measures the strength of the interband optical transitions, as was discussed in the absorption coefficient analysis, while the second one measures the normal oscillation of the atoms.

The value of $\frac{1}{n(E)^2 - 1}$ is founded and plotted as a function of E^2 for all 6 films and was showed in figure (4.12). In order to find the oscillator parameters, E_d and E_0 we can write equation (4.5) in another shape as follow,

$$\frac{1}{n(E)^2 - 1} = \frac{E_0}{E_d} - \frac{E^2}{E_d E_0} \quad (4.6)$$

it is clear that the relation between $\frac{1}{n(E)^2 - 1}$ and E^2 is linear one, where the slope of that line will represent the value of $\frac{1}{E_d E_0}$ and the intersection with y-axis represents the value of $\frac{E_0}{E_d}$. We can derive the value of E_d

from the slope and the intersection with y-axis of the straight line Fig. (4.12) i.e, $E_d = \sqrt{\frac{1}{(\text{the slope}) \times (\text{y-intercept})}}$, these calculation were carried

out by using Excel program where the value of E_d was founded, for all our films, and are showed in Table. (4.4).

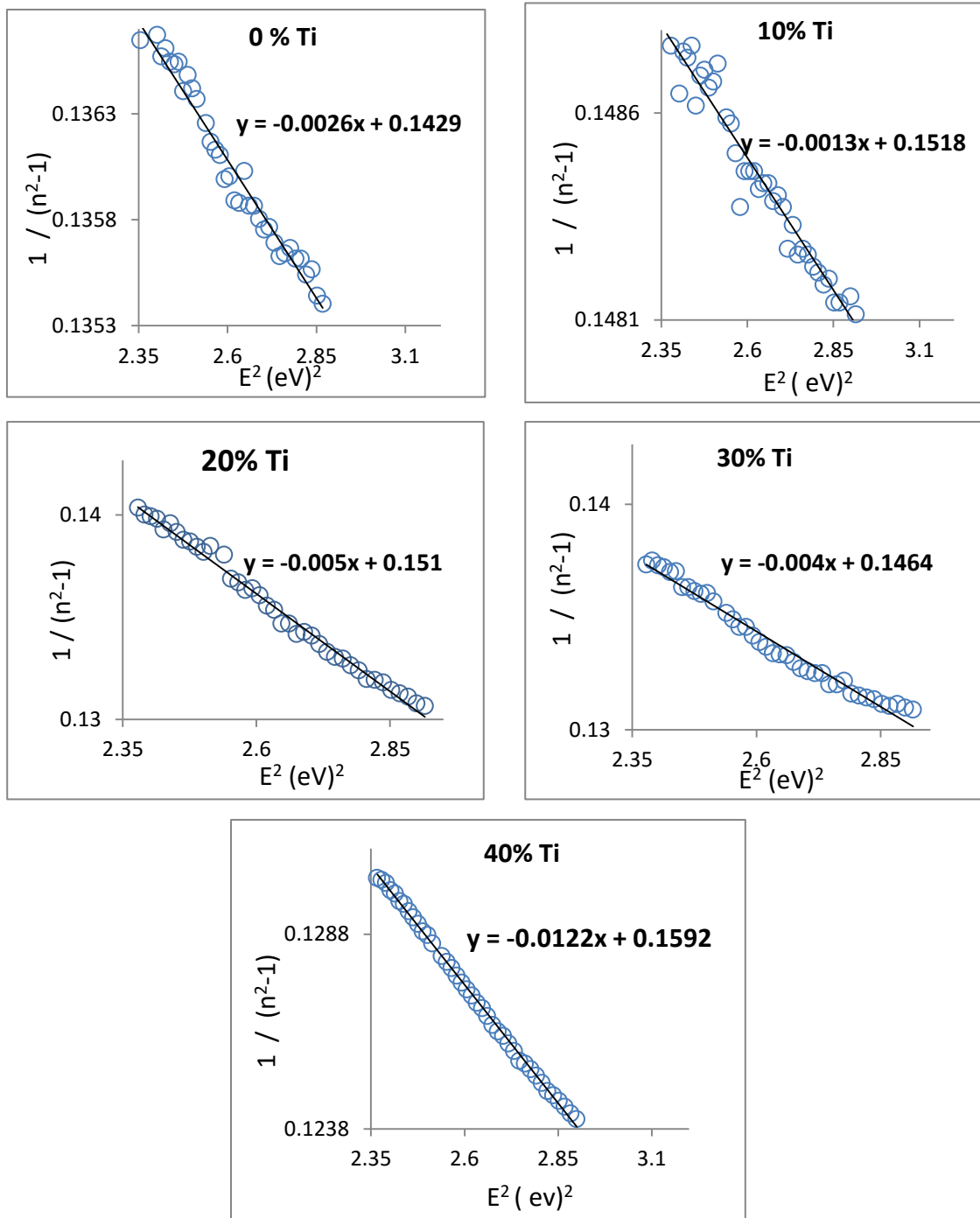


Fig 4.12: The value of $\frac{1}{n(E)^2-1}$ as a function of E^2 of WO₃ thin film at different Ti concentrations.

Table. 4.4 : The dispersion energy E_d , the oscillator energy E_0 , the lattice dielectric constant ϵ_L and the static refractive index ϵ_s of WO_3 thin films doped with Ti at deferent concentrations.

Ti (%)	E_d (eV)	E_0 (eV)	ϵ_s	ϵ_L
0	51.88	7.41	8.00	8.10
10	71.19	10.80	7.59	7.89
20	36.39	5.50	7.62	9.13
30	41.38	6.04	7.85	8.91
40	22.69	3.61	7.28	10.90

The static refractive index is also evaluated from relation (4.5), i.e., if we find (y-axis intercept multiple by E_d) this will be the value of E_0 , these calculations were also done by using Excel program and are showed in table (4.5). The value of the static dielectric constant was founded by using relation (4.5), where $n^2(E = 0) = 1 + \frac{E_d}{E_0}$, and the obtained values are showed in Table (4.5). From the static and dispersion energies we can say in general that these films can be used as sensors for all kinds of UV, while WO_3 doped with 10% Ti will be the best one because it has the highest oscillator energy which means the highest ability of energy storage.

In addition, we can find the lattice dielectric constant (ϵ_L) from the refractive index (n) by this relation [114],

$$n^2 = \epsilon_l - A\lambda^2 \quad (4.7)$$

Where A is a constant. By plotting n^2 as a function of λ^2 we were able to determine the lattice dielectric constant, ϵ_L , by fitting a linear function using equation (4.7), where the value of, ϵ_L , will be the intercept of the slope of that solid. The fitting of the above reported function is illustrated in figure 4.11, for all samples under investigation.

The values of ϵ_L of the investigated WO_3 : Ti doped films are calculated and are shown in Table (4.4). The lattice dielectric constant of WO_3 thin film doesn't change when doped with 10% Ti and so the crystal structure of WO_3 thin film and WO_3 doped with 10% Ti thin films are the same and also the same desirable electrochromic properties. However for higher concentrations of Ti we note that ϵ_L increases, which indicates that the lattice parameters changes at higher Ti concentrations due to the formation of TiO_2 that we expected to be formed at higher Ti concentrations.

The estimation of the dispersion parameters is of importance in the technological applications of materials. At high dispersion energies free carriers couples with electrons of the outermost shell of atoms or molecules of this material. This results in electric polarization resonance, relaxation and energy storage and dissipation. On the other hand, the difference in the values of lattice and static dielectric constants is ascribed to the free carriers contribution. The total dielectric function ($\epsilon_{eff} = \epsilon_0 + \delta\epsilon_l + \delta\epsilon_e$) is composed of that of free space (ϵ_e) to the dielectric function. The symbol δ in the equation refers to small variation. The electronic contribution includes the free carriers and the entire set of valence electrons [115]. As the dielectric constant depends on the frequency of the incident light, the response of electrons and the lattice to the time varying light wave depends on the frequency value [116]. In the absence of free carriers, the permittivity approaches the static value. This explains the reason beyond the very slight variation in (ϵ_s) and the strong variation in (ϵ_l). Because our calculated dispersive parameters are not calculated in the literature yet (to our knowledge), we were not able to compare them with others.

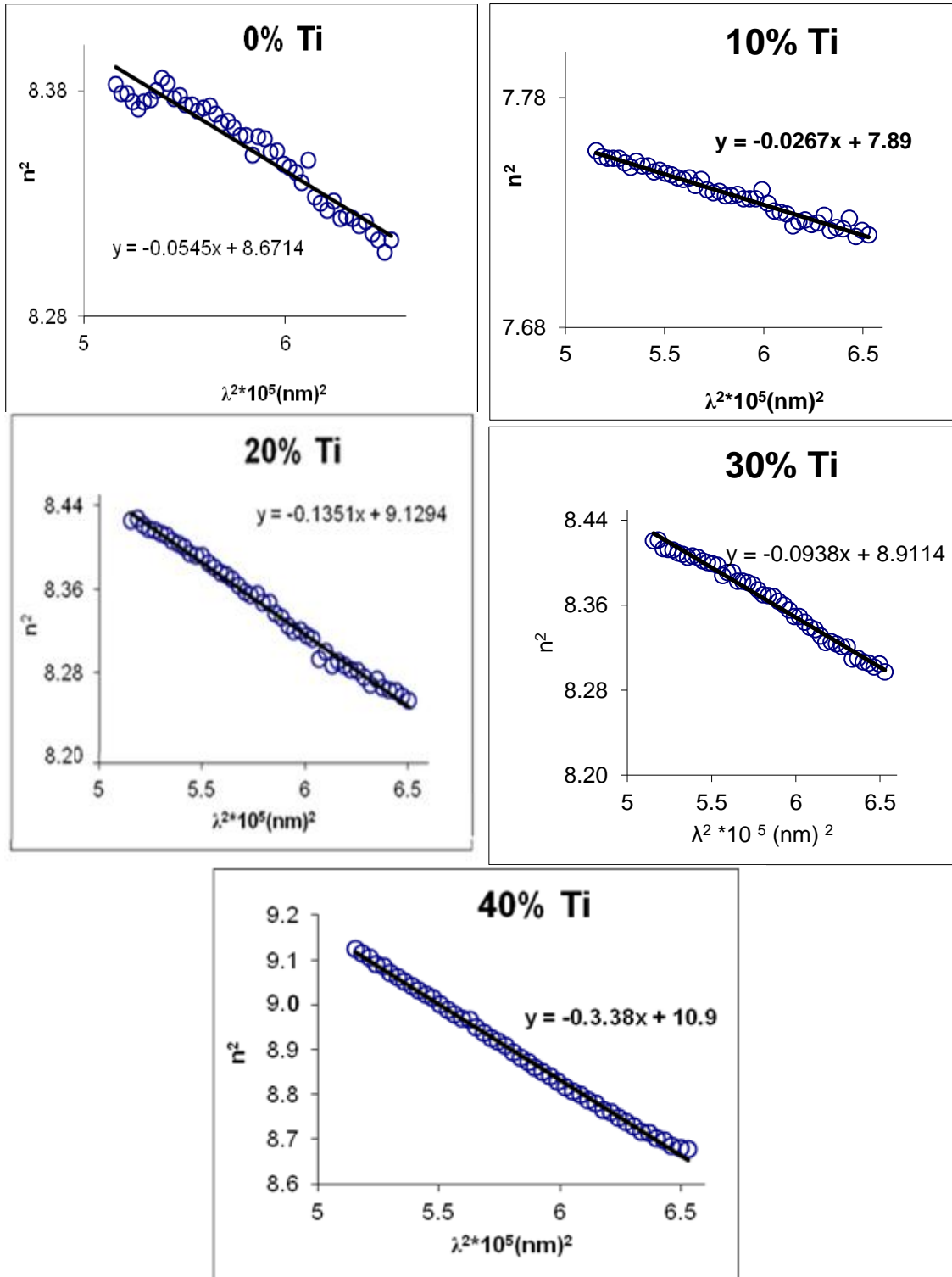


Fig 4.13: The value of n^2 versus λ^2 of WO₃:Ti doped thin film at specific concentrations.

Conclusion

WO₃ thin films doped with Ti were successfully synthesized by dipping a well cleaned glass substrate in a sol-gel. The sol – gel was prepared by adding certain weights of WCl₆ with TiCl₂ with glycerol and ethanol where the mixing process was carried out by ultrasonic water bath at 25°C . The films finally were heated at 160°C.

The crystal structure of the prepared films was revealed by XRD to be an amorphous one. The optical constants and optical band gaps of the prepared films have also been studied from the absorption coefficient which gave a direct allowed transition band gap of 3.1eV. Due to this large energy gap, all the samples showed an increased transparency with increasing the incident wavelength. It is also found that the energy gap of WO₃ decreased when doped with 10% Ti due to the energy levels that introduced in that gap while it increased slightly up to 3.6 eV with increasing Ti concentration. This is due formation of TiO₂ new phase that may be formed in the amorphous structure. The same tendency was found in the reflectance, as in the energy gap, this is further evidence that a new phase might be formed in the amorphous structure (TiO isolator phase).

Both the thickness and the dielectric constant were calculated from the reflectance spectra, and it was found that the thickness of films increased with increasing doping concentration from 0.373 μm to almost a constant value (≈ 0.7μm) which can be attributed to the increases in the liquid viscosity as the doped concentration increasing.

The dielectric constant increases with increasing the Ti doping concentration, this is also due to the formation TiO_2 phase that has an insulating nature.

From the refractive index the oscillator energies, static dielectric constant and static refractive index of these films were identified which show that WO_3 thin films doped with Ti can be used as UV sensors, where 10% Ti doping is the best sensor.

References

- [1] Rolf E. Hummel and Karl H. Guenther, "**Thin Films for Optical Coatings**", Volume 1, CRC Press LLC, 111, (1995).
- [2] M. C. RAO, "*Structure And Properties of WO₃ Thin Films for Electrochromic Device Application*", **Journal of Non-Oxide Glasses**, 5(1), 1-8, (2013).
- [3] C. Cantalinia, H.T. Suna, M. Facciob, M. Pelinoa, S. Santuccic, L. Lozzic and M. Passacantandoc, "*NO₂ sensitivity of WO₃ thin film obtained by high vacuum thermal evaporation*", **Sensors and Actuators B: Chemical**, 31(1-2), 81-87, (1996).
- [4] Joel Díaz-Reyes, Roberto Castillo-Ojeda, Miguel Galván-Arellano and Orlando Zaca-Moran, "**Characterization of WO₃ Thin Films Grown on Silicon by HFMOD**", *Advances in Condensed Matter Physics*, 2013, 1-9, (2013).
- [5] Chang-Yeoul Kima,* , Seong-Geun Cho, Seok Park and Duck-Kyun Choi, "*Tungsten oxide film synthesis by spray pyrolysis of peroxotungstic acid and its electrochromic characterization*", **Journal of Ceramic Processing Research**, 10(6), 851-854 (2009).
- [6] Rishabh Jain¹, Yang Wang and Radenka Maric, "*Tuning of WO₃ Phase Transformation and Structural Modification by Reactive Spray Deposition Technology*", **J Nanotech Smart Mater**, 1(203), 1-7, (2014).
- [7] Wei-Han Tao, and Ching-Hsiang Tsai, "**H₂S sensing properties of noble metal doped WO₃ thin film sensor fabricated by**

- micromachining", **Sensors and Actuators B: Chemical**, 81(2–3), 237–247, (2002).
- [8] A. Rampaula, I. Parkina, S. O'Neill, J. DeSouza and A. Mills, N. Elliott, *"Titania and tungsten doped titania thin films on glass; active photocatalysts"*, **Polyhedron**, 22(1), 35-44, (2003).
- [9] A. Shengelaya, S. Reich, Y. Tsabba and K.A. Müller, *"Electron spin resonance and magnetic susceptibility suggest superconductivity in Na doped WO₃ samples"*, **The European Physical Journal B - Condensed Matter and Complex Systems**, 12 (1), 13-15, (1999).
- [10] F. Paulo Rouxinol, B. Cláudio Trasferetti, Richard Landers and Mário A. Bica de Moraes, *"Hot-filament metal oxide deposition (HFMOD): a novel method for depositing thin films of metallic oxides"*, **J. Braz. Chem. Soc.** 15 (2), (2004).
- [11] A. G. Souza Filho, J. Mendes Filho, V. N. Freire, A. P. Ayala, J. M. Sasaki, P. T. C. Freire, F. E. A. Melo, J. F. Juliao and U. U. Gomes, *"Phase transition in WO₃ microcrystals obtained by sintering process"*, **J. Raman Spectrosc.**, 32, 695–699, (2001).
- [12] Ekhard K H Salje, Stephan Rehm, Frank Pobell, Darryl Morris, Kevin S Knight, Thomas Herrmannsdörfer and Martin T Dove, *"Crystal structure and paramagnetic behaviour of ε - WO_{3-x}"*, **Journal of Physics: Condensed Matter** 9(31), 6563-6578, (1997).
- [13] Xiaosheng Fang, Yoshio Bando, Ujjal K. Gautam, Changhui Ye and Dmitri Golberg, *"Inorganic*

- semiconductor nanostructures and their field-emission applications"*, **Journal of Materials Chemistry**, 5, (2008).
- [14] Zhifu Liu, Toshinai Yamazaki, Yanbai Shen, Toshio Kikuta and Noriyuki Nakatani, "*Influence of annealing on microstructure and NO₂-sensing properties of sputtered WO₃ thin films*", **Sensors and Actuators B: Chemical**, 128 (1), 173–178, (2007).
- [15] Satyen K. Deb, "*Opportunities and challenges in science and technology of WO₃ for electrochromic and related applications*", **Solar Energy Materials and Solar Cells**, 92 (2), 245–258, (2008).
- [16] Ji-yan Leng, Xiu-juan Xu, Ning Lv, Hui-tao Fan, Tong Zhang, "*Synthesis and gas-sensing characteristics of WO₃ nanofibers via electrospinning*", **Journal of Colloid and Interface Science** 356, 54–57, (2011).
- [17] Bin Ding, Moran Wang, Jianyong Yu and Gang Sun, "*Gas Sensors Based on Electrospun Nanofibers*", **Sensors** 9, 1609-1624, (2009).
- [18] K. Memarzadeh, M. Vargas, J. Huang, J. Fan, R.P. Allaker, "*Nano Metallic-Oxides as Antimicrobials for Implant Coatings*", **Key Engineering Materials**, 493-494, 489-494, (2011).
- [19] Hyoungh-il Kim, Jungwon Kim, Wooyul Kim, and Wonyong Choi, "*Enhanced Photocatalytic and Photoelectrochemical Activity in the Ternary Hybrid of CdS/TiO₂/WO₃ through the Cascaded Electron Transfer*", **J. Phys. Chem. C**, 115 (19), 9797–9805, (2011).

- [20] Tetsu Tatsuma , Shuichi Saitoh, Pailin Ngaotrakanwivat , Yoshihisa Ohko, and Akira Fujishima, " *Energy Storage of TiO_2-WO_3 Photocatalysis Systems in the Gas Phase*", *Langmuir*, 18 (21), 7777–7779, (2002).
- [21] Jia Hong Pan and Wan In Lee, " *Preparation of Highly Ordered Cubic Mesoporous WO_3/TiO_2 Films and Their Photocatalytic Properties*", *Chem. Mater.*, 18 (3), 847–853, (2006).
- [22] Dandan Song, Zhao Chen, Peng Cui, Meicheng Li, Xing Zhao, Yaoyao Li, and Lihua Chu, " *NH_3 -treated WO_3 as low-cost and efficient counter electrode for dye-sensitized solar cells*", *Nanoscale Res Lett*, 10, (2015).
- [23] Hamilton Varela, Fritz Huguenin and Marcos Malta e Roberto M. Torresi, " *MATERIAIS PARA CÁTODOS DE BATERIAS SECUNDÁRIAS DE LÍTIO*", *Quím. Nova* 25(2), 287-293, (2002).
- [24] B. Cláudio Trasferetti , F. Paulo Rouxinol , Rogério V. Gelamo , and Mário A. Bica de Moraes, " *Berreman Effect in Amorphous and Crystalline WO_3 Thin Films*", *J. Phys. Chem. B*, 108 (33), 12333–12338, (2004).
- [25] S. Ma and B. G. Frederick , " *Reactions of Aliphatic Alcohols on $WO_3(001)$ Surfaces*", *J. Phys. Chem. B*, 107 (43), 11960–11969, (2003).
- [26] M.Z. Ahmad, J.H. Kang, A.Z. Sadek, A. Moafi, G. Sberveglieri and W. Wlodarski, " *Synthesis of WO_3 Nanorod based Thin Films for*

- Ethanol and H₂Sensing"**, **Procedia Engineering** 47, 358–361, (2012).
- [27] Li Min Kuo, Yu-Tai Shih, Cen-Shawn Wu, Yu-Chi Lin and Shuchi Chao, "*A new hybrid method for H₂S-sensitive devices using WO₃-based film and ACF interconnect*", **Measurement Science and Technology**,24(7), (2013).
- [28] Nguyen Van Hieu, Dang Thi Thanh Le, Nguyen Duc Khoang, Nguyen Van Quy, Nguyen Hoa, Phuong Tam, Anh-Tuan Le and Tran Trung, "*A comparative study on the NH₃ gas-sensing properties of ZnO, SnO₂, and WO₃ nanowires*", **Int J Nanotechnol** 8, 174-187, (2011).
- [29] Guerin J, Bendahan A, Aguir K, "*A dynamic response model for the WO₃-based ozone sensors*", **Sensor Actuat B-Chem** 128, 462-467, (2008).
- [30] Al-Kuhaili MF, Durrani SMA, Bakhtiari IA, "*Carbon monoxide gassensing properties of CeO₂-WO₃ thin films*", **Mater Sci Tech**, 26, 726-731, (2010).
- [31] Huige Wei, Xingru Yan, Yunfeng Li, Hongbo Gu, Shijie Wu, Keqiang Ding, Suying Wei, and Zhanhu Guo, "*Electrochromic Poly(DNTD)/WO₃ Nanocomposite Films via Electropolymerization*", **J. Phys. Chem. C**, 116 (30),16286–16293, (2012).
- [32] Kihyon Hong, Kisoo Kim, Sungjun Kim, Illhwan Lee, Hyunsu Cho, Seunghyup Yoo, Ho Won Choi, Nam-Yang Lee, Yoon-Heung

- Tak, and Jong-Lam Lee, "*Optical Properties of WO₃/Ag/WO₃ Multilayer As Transparent Cathode in Top-Emitting Organic Light Emitting Diodes*", *J. Phys. Chem. C*, 115 (8), 3453–3459, (2011).
- [33] Sumeet Walia, Sivacarendran Balendhran, Hussein Nili, Serge Zhuiykov, Gary Rosengarten, Qing Hua Wang, Madhu Bhaskaran, Sharath Sriram, Michael S. Strano and Kourosh Kalantar-zadeha, "*Transition metal oxides- thermoelectric properties*", *Progress in Materials Science*, 58(8), 1443-1489, (2013).
- [34] Sibuyi, P. "*Nano-rods WO_{3-δ} for electrochromic smart windows applications*", (Doctoral dissertation, University of Western Cape), 25, (2006).
- [35] C. V. Ramana , S. Utsunomiya , R. C. Ewing , C. M. Julien , and U. Becker , "*Structural Stability and Phase Transitions in WO₃ Thin Films*", *J. Phys. Chem. B*, 110 (21), 10430–10435, (2006).
- [36] I. Jiménez, , J. Arbiol, G. Dezanneau, A. Cornet and J.R. Morante, "*Crystalline structure, defects and gas sensor response to NO₂ and H₂S of tungsten trioxide nanopowders*", *Sensors and Actuators B: Chemical*, 93, (1–3), 475–485, (2003).
- [37] C. V. Ramana , Gaurav Baghmar , Ernesto J. Rubio , and Manuel J. Hernandez, "*Optical Constants of Amorphous, Transparent Titanium-Doped Tungsten Oxide Thin Films*", *ACS Appl. Mater. Interfaces*, 5 (11), pp 4659–4666, (2013).

- [38] Suvarna R Bathe and P S Pati, "*Influence of Nb doping on the electrochromic properties of WO₃ films*", **J. Phys. D: Appl. Phys.** 40 7423, (2007).
- [39] Dong Won Hwang, Jindo Kim, Tae Jin Park, Jae Sung Lee, "*Mg-Doped WO₃ as a Novel Photocatalyst for Visible Light-Induced Water Splitting*", **Catalysis Letters**, 80(1-2), 53-57, (2002).
- [40] Tao Zhu, Meng Nan Chon and Eng Seng Chan, "*Nanostructured Tungsten Trioxide Thin Films Synthesized for Photoelectrocatalytic Water Oxidation: A review*", **ChemSusChem**, 7, 2974 – 2997, (2014).
- [41] Tao He, Ying Ma, Ya-an Cao, Wen-sheng Yang and Jian-nian Yao, "*Improved photochromism of WO₃ thin films by addition of Aunanoparticles*", **Phys. Chem. Chem. Phys.**, 4, 1637-1639, (2002).
- [42] Suvarna R. Bathe and P.S. Patil, "*Titanium doping effects in electrochromic pulsed spray pyrolysed WO₃ thin films*", **Solid State Ionics**, 179, 314–323, (2008).
- [43] Suvarna R. Bathe and P. S. Patil, "*Electrochemical Behavior of TiO₂ Nanoparticle Doped WO₃ Thin Films*", **Journal of Materials**, 2014, Article ID 642069, 5 pages, (2014)
- [44] Sofian M. Kanan, Oussama M. El-Kadri, Imad A. Abu-Yousef and Marsha C. Kanan, "*Semiconducting Metal Oxide Based Sensors for Selective Gas Pollutant Detection*", **Sensors**, 9(1424-8220), 8158-8196, (2009).

- [45] Chandra Roychoudhuri, A.F. Kracklauer and Kathy Creath, *"The Nature of Light: What is a Photon?"*, CRC Press, 3-4, (2008).
- [46] James W. Robinson, Eileen M. Skelly Frame and George M. Frame II, *"Undergraduate Instrumental Analysis"*, CRC Press, Sixth Edition, 65-66, (2004).
- [47] Barry G. Hinwood, *"A Textbook of Science for the Health Professions"*, Nelson Thornes, 2nd ed, 121-122, 1997.
- [48] Jennifer Hill, *"Excel HSC & Preliminary Senior Science"*, Pascal Press, 118-119, (2002).
- [49] Ann Fullick and Patrick Fullick, *"Physics for AQA.: Separate award"*, Heinemann, 48-49, (2001).
- [50] Andrew Burrows, John Holman, Andrew Parsons, Gwen Pilling and Gareth Price, *"Chemistry³: Introducing Inorganic, Organic and Physical Chemistry"*, Oxford University Press, 2nd ed, 447, (2013).
- [51] Julius Adams Stratton, *"Electromagnetic Theory"*, John Wiley & Sons, 1-12, (2007).
- [52] Weng Cho Chew, Mei Song Tong and Bin Hu, *"Integral Equation Methods for Electromagnetic and Elastic Waves"*, Morgan & Claypool Publishers, ,(2009).
- [53] T. K. Sarkar, Michael C. Wicks, M. Salazar-Palma and Robert J. Bonneau, *"Smart Antennas"*, John Wiley & Sons, 11-15, (2005).

- [54] T. K. Sarkar, Michael C. Wicks, M. Salazar-Palma, Robert J. Bonneau, *"Smart Antennas"*, John Wiley & Sons, 1-112, (2005).
- [55] Martin Dressel and George Grüner, *"Electrodynamics of Solids: Optical Properties of Electrons in Matter"*, Cambridge University Press, 1st ed, 10-15, (2002).
- [56] Pankaj K. Das, *"Lasers and Optical Engineering"*, Springer Science & Business Media, 75-76, (2012).
- [57] S Gupta, *"Krishan's Engineering Physics II"*, Krishna Prakashan Media, 17th ed 1-4, (2010).
- [58] MARK FOX, *"Optical Properties of Solids"*, Oxford University Press, 1st ed, 1-7, (2001).
- [59] Rajiv Chopra, *"Computer Graphics: A Practical Approach, Concepts, Principles, Case Studies, Experiments (For B E/BTech, BCA & MCA Courses)"*, S. Chand, 396-397, (2011).
- [60] George Arfken, *"University Physics"*, Academic Press, 755-757, (2012).
- [61] James W. Robinson, Eileen M. Skelly Frame and George M. Frame II, *"Undergraduate Instrumental Analysis"*, CRC Press 6th, 65-70, (2004).
- [62] Settimio Mobilio, Federico Boscherini and Carlo Meneghini, *"Synchrotron Radiation: Basics, Methods and Applications"*, Springer, 107-109, (2014).
- [63] Steve Holzner, *"Physics For Dummies"*, John Wiley & Sons, 324-326, (2006).

- [64] John Kenkel, "*Analytical Chemistry for Technicians*", Fourth Edition, CRC Press, 190, (2013).
- [65] G Vijayakumari, "*Engineering Physics, 2E*", Vikas Publishing House 347, (2009).
- [66] Richard S. Quimby, "*Photonics and Lasers: An Introduction*", John Wiley & Sons, 11-14, (2006).
- [67] Changhoon Choi, "*Kinetic Study of Copper Chemistry in Chemical Mechanical Polishing (CMP) by an In-situ Real Time Measurement Technique*", ProQuest, 115-117, (2008).
- [68] Dennis Goldstein and Dennis H. Goldstein, "*Polarized Light, Revised and Expanded*", CRC Press, 133-139, (2003).
- [69] Dennis H. Goldstein, "*Polarized Light*", CRC Press, 3rd ed, 117-124, (2010).
- [70] Helmut H. Telle, Angel González Ureña, Robert J. Donovan, "*Laser Chemistry: Spectroscopy, Dynamics and Applications*", John Wiley & Sons, 152, (2007).
- [71] Erik Reinhard, Erum Arif Khan, Ahmet Oguz Akyuz and Garrett Johnson, "*Color Imaging: Fundamentals and Applications*", CRC Press, 24-30, (2008).
- [72] Kai-Erik Peiponen, Erik M. Vartiainen and Toshimitsu Asakura, "*Dispersion, Complex Analysis and Optical Spectroscopy: Classical Theory*", Springer Science & Business Media, 11-13, (1999).

- [73] Jerry C. Whitaker , "*The Electronics Handbook*", CRC Press, 113, (1996).
- [74] W. H. Strehlow and E. L. Cook, "*Compilation of Energy Band gaps in Elemental and Binary Compound Semiconductors and Insulators*", J. Phys. Chem. Ref. 2(1), 163-199, (1973).
- [75] Michael A. Parker, "*Solid State and Quantum Theory for Optoelectronics*", CRC Press, 10-14, (2009).
- [76] Yehuda B. Band, "**Light and Matter: Electromagnetism, Optics, Spectroscopy and Lasers**", John Wiley and Sons Ltd,88-98, (2007).
- [77] H. C. Casey Jr., D. D. Sell, and K. W. Wecht, "*Concentration dependence of the absorption coefficient for n- and p- type GaAs between 1.3 and 1.6 eV*", The Journal of Applied Physics, 46, 250-257, (1975).
- [78] T. S. Kayed, A. F. Qasrawi, and Khaled A. Elsayed, "*Optical characterization of the MgO/InSe interface*", Phys. Status Solid B, 252(3), 621–625, (2015).
- [79] R. I. Pankove, "*Optical properties in semiconductors*", Printice-Hall international, Englewood Clifts, New Jersey, 1971.
- [80] Nader Ghobadi, "*Band gap determination using absorption spectrum fitting procedure*", International Nano Letters Ghobadi; licensee Springer, 3(2), 1-4, (2013).
- [81] Kwan Chi Kao, "*Dielectric Phenomena in Solids*", Academic Press, 127, (2004).

- [82] S. Mani Naidu, Naidu S. Mani, "*Applied Physics*", Pearson Education, 6-20, (2009).
- [83] Safa Kasap and Peter Capper, "*Springer Handbook of Electronic and Photonic Materials*", Springer Science & Business Media, 48-51, (2006).
- [84] By Yun Lu, Liang Hao and Hiroyuki Yoshida, "*Mechanical Coating Technique for Composite Films and Composite Photocatalyst Films*", INTECH Open Access Publisher, 303, (2012).
- [85] Kiyotaka Wasa, "**Handbook of Sputter Deposition Technology: Fundamentals and Applications for Functional Thin Films, Nano-materials and MEMS**", William Andrew, 14-25, (2012).
- [86] Reza Ghodssi and Pinyen Lin, "*MEMS Materials and Processes Handbook*", Springer Science & Business Media 142-145, (2011).
- [87] Guy Rabilloud, "*High-Performance Polymer*", Editions OPHRYS 239-240,
- [88] Sam Zhang, "*Nanostructured Thin Films and Coatings: Mechanical Properties*", CRC Press, 160-162, (2010).
- [89] D. Widmann, H. Mader, H. Friedrich, "*Technology of Integrated Circuits*", Springer Science & Business Media, 33, (2000).
- [90] Todd D. Steiner, "*Semiconductor Nanostructures for Optoelectronic Applications*", Artech House, 31-34, (2004).
- [91] Joseph Shinar, "*Organic Light-Emitting Devices: A Survey*", Springer Science & Business Media, 10, (2004).

- [92] "*Vacuum Physics and Technology*" , Academic Press, 521-523, (1980).
- [93] Lifeng Chi, "*Nanotechnology: Volume 8: Nanostructured Surfaces*", John Wiley & Sons, 21-23, (2010).
- [94] S Tabatabaei, A Shukohfar , R Aghababazadeh and A Mirhabibim, "*Experimental study of the synthesis and characterisation of silica nanoparticles via the sol-gel method*", Journal of Physics: Conference Series 26, 371–374, (2006).
- [95] C. Jeffrey Brinker and George W. Scherer, "*Sol-gel Science: The Physics and Chemistry of Sol-gel Processing*", Gulf Professional Publishing, 1-2, (1990).
- [96] Guocheng Wang and Hala Zreiqat, "*Functional Coatings or Films for Hard-Tissue Applications* ", Materials, 3, 3994-4050, (2010).
- [97] Lisa C. Klein, "*Sol-Gel Optics: Processing and Applications*", Springer Science & Business Media, 15-17, (2013).
- [98] Alain C. Pierre, "*Introduction to Sol-Gel Processing*", Springer Science & Business Media, 1-5, 2013
- [99] Michel A. Aegerter and M. Mennig, "*Sol-Gel Technologies for Glass Producers and Users*", Springer Science & Business Media, 37-40, (2013).
- [100] P. Yimsiri and M.R. Mackley, "*Spin and dip coating of light-emitting polymer solutions: Matching experiment with modeling*", Chemical Engineering Science 61 3496 – 3505, (2006).

- [101] H. C. Mayer and R. Krechetnikov, "*Landau-Levich flow visualization: Revealing the flow topology responsible for the film thickening phenomena*", PHYSICS OF FLUIDS, 24, 052103, (2012).
- [102] B. Guzeldir, M. Saglam and A. Ates, "*Deposition and Characterization of CdS, CuS and ZnS Thin Films Deposited by SILAR Method*", ACTA PHYSICA POLONICA, 121, (2012).
- [103] Vyshnavi Narayanan, Els Bruneel , Ruben Hühne and Isabel Van Driessche, "*Dip-Coating of Water-based Buffer Layers: An X-ray Photoelectron Spectroscopy Study*", Nanomaterials, 2, 251-267, (2012).
- [104] Algirdas LAZAUSKAS and Viktoras GRIGALI-NAS, "*Float Glass Surface Preparation Methods for Improved Chromium Film Adhesive Bonding*", MATERIALS SCIENCE, 18 (2), (2012).
- [105] Hyun-Wook Ryu_ and Kyung-Hee Park, "*Synthesis and Characterization of WO₃ Nanopowders and Their Electrical Properties*", Journal of the Korean Physical Society, 42 (6), 727-730, (2003).
- [106] Nilgun Ozer and Nilgun Dogan, "*Study of electrochromism in Ti:WO₃ films by sol-gel process*", SPIE Proceedings, 3424, 106-114, (2013).
- [107] Suvarna R. Bathe, and P.S. Patil, "*Titanium doping effects in electrochromic pulsed spray pyrolysed WO₃ thin films*", Solid State Ionics, 179(9-10), 314-323, (2008).

- [108] Esra Ozkana, Se-Hee Lee, C.Edwin Tracy, J.Roland Pitts and Satyen K. Deb, "*Comparison of electrochromic amorphous and crystalline tungsten oxide films*", Solar Energy Materials and Solar Cells, 79(4), 439–448, (2003).
- [109] NilgUn Ozer adNilgUn Doan, "*Study of electrochromism in Ti:W03 films by solgel process*", SPIE, 3424, 106-114, , (1998)
- [110] Rao M.C. and Hussain O.M , "*Optical Properties of Vacuum Evaporated WO₃ Thin Films*", Res.J.Chem.Sci., 1(7), 76-80, (2011)
- [111] Hongbin Wu and Lai-Sheng Wang, "*The electronic structure of titanium oxide clusters: TiO_y (y = 1-3) and (TiO₂)_n (n = 1-4)*", chem. phys., 107 (20), 8221, (1997).
- [112] C. W. Walter, C. F. Hertler, P. Devynck, G. P. Smith, J. R. Peterson, "*Photodetachment of WO-3: The electron affinity of WO₃*", J. Cham. Phys., 95(2), 824, (1991).
- [113] M. G. Cohen, M. DiDomenico Jr., S. H. Wemple, "*Theory of the Elasto-Optic Effect in Nonmetallic Crystals*", Phys. Rev. B1, 4334-4337, (1970).
- [114] M. Dresselhaus, "*Optical Properties of Solids*", American Scientific Publishers, New York, 110-130, (1980).
- [115] D. K. Ferry, "*Semiconductor Transport*", London, Taylor & Francis, (2000).
- [116] Joseph R. Lakowicz, "*Principles of Fluorescence Spectroscopy*", 3rd edition, Baltimore, Spring, (2010).

جامعة النجاح الوطنية
كلية الدراسات العليا

فجوة الطاقة الضوئية و الثوابت الضوئية لأفلام ثالث أكسيد
النتجستن الرقيقة المطعمة بالتيتانيوم بطريقة التغليف
بالغمس في السائل الهلامي (So-gel)

إعداد

منار ابراهيم علي شواهنة

إشراف

د. اياد سعد الدين

د. محمد سليمان

قدمت هذه الأطروحة استكمالاً لمتطلبات الحصول على درجة الماجستير في الفيزياء بكلية
الدراسات العليا في جامعة النجاح الوطنية في نابلس، فلسطين.

2015

ب

فجوة الطاقة الضوئية و الثوابت الضوئية لأفلام ثالث أكسيد التنجستن الرقيقة المطعمة بالتيتانيوم بطريقة التغليف بالغمس في السائل الهلامي (So-gel)

إعداد

منار ابراهيم علي شواهنة

إشراف

د. اياد سعد الدين

د. محمد سليمان

الملخص

باستخدام طرق التشخيص الضوئية، تم فحص الثوابت الضوئية وفجوة الطاقة لأفلام ثلاثي أكسيد التنجستن (WO_3) الرقيقة، المحضرة بطريقة التغليف بالغمس في المحلول الهلامي (sol – gel) على الزجاج. تم ايجاد بناء غير بلوري لجميع الأفلام المسخنة على درجة حرارة 160° س باستخدام (XRD). كشفت البيانات الضوئية أن فجوة الطاقة لهذه الأفلام هي فجوة من نوع الانتقال المباشر المسموح به و قيمتها (3.1 e.v)، حيث وجد أن هذه الفجوة تزداد مع زيادة تركيز عنصر التيتانيوم (Ti) حتى 3.6 e.v وذلك ربما يكون بسبب تكون مركب ثنائي أكسيد التيتانيوم (TiO_2) في داخل التركيب غير البلوري. تم اختبار تأثير تركيز التيتانيوم (Ti) على سُمك الأفلام وعلى الثوابت الضوئية التي تشمل (معامل الانكسار الضوئي للوسط وثابت الامتصاصية وثابت العزل الكهربائي). وُجد أن سُمك الافلام يزداد مع زيادة تركيز التطعيم من $0.373\mu m$ الى تقريباً قيمة ثابتة وهي $0.7\ \mu m$ وذلك بسبب زيادة لزوجة السائل كما هو متوقع. معامل الانكسار للوسط عند درجة حرارة الغرفة والذي تم حسابه من بيانات الانعكاسية والنفاذية، سمح في ايجاد كل من طاقة التشتت وطاقة الاهتزاز وثابت العازلية الثابت وثابت العازلية الشبكي.